# Mutations in the Bone Morphogenetic Protein signaling pathway sensitize zebrafish and humans to ethanol-induced jaw malformations

John R. Klem[1], Tae-Hwi Schwantes-An[2], Marco Abreu[2], Michael Suttie[3,4], Raeden Gray[1], Hieu Vo[1], Grace Conley[1], Tatiana M. Foroud[2], Leah Wetherill[2], CIFASD, and C. Ben Lovely[1*].

[1]University of Louisville School of Medicine, Department of Biochemistry and Molecular Genetics, Alcohol Research Center, Louisville, KY. [2]Department of Medical and Molecular Genetics, Indiana University School of Medicine, Indianapolis, IN. [3]Nuffield Department of Women's and Reproductive Health, University of Oxford, Oxford, United Kingdom. [4]Big Data Institute, University of Oxford, Oxford, United Kingdom.

* correspondence to: ben.lovely@louisville.edu

**Abstract**

Fetal Alcohol Spectrum Disorders (FASD) describe ethanol-induced developmental defects including craniofacial malformations. While ethanol-sensitive genetic mutations contribute to facial malformations, the impacted cellular mechanisms remain unknown. Bmp signaling is a key regulator of epithelial morphogenesis driving facial development, providing a possible ethanol-sensitive mechanism. We found that zebrafish mutants for Bmp signaling components are ethanol-sensitive and affect anterior pharyngeal endoderm shape and gene expression, indicating ethanol-induced malformations of the anterior pharyngeal endoderm cause facial malformations. Integrating FASD patient data, we provide the first evidence that variants in the human Bmp receptor gene *BMPR1B* associate with ethanol-related differences in jaw volume. Our results show that ethanol exposure disrupts proper morphogenesis of, and tissue interactions between, facial epithelia that mirror overall viscerocranial shape changes and are predictive for Bmp-ethanol associations in human jaw development. Our data provide a mechanistic paradigm linking ethanol to disrupted epithelial cell behaviors that underlie facial defects in FASD.

**Keywords:** Fetal Alcohol Spectrum Disorders, Zebrafish, Alcohol, Genetics, FASD, Endoderm, Jaw development.

## Introduction

Ethanol is the most common environmental risk factor for congenital anomalies, with Fetal Alcohol Spectrum Disorders (FASD) describing all ethanol-induced birth defects. Global estimated incidence rates of FASD are .77%, though subpopulations of FASD can be much higher, ranging from 2-5% in the US and nearly 30% of individuals in some parts of the world with higher incidences of binge drinking (1,2). However, these numbers may be underestimates as nearly half of all pregnancies in the US are unplanned, and many pediatricians fail to recognize FASD (3,4). Highly variable, multiple phenotypes present with FASD include structural malformations to the brain and face (5). At the most severe end of the FASD spectrum is Fetal Alcohol Syndrome (FAS), which frequently presents as craniofacial defects including jaw hypoplasia (6). However, increasing data indicates that prenatal alcohol exposure (PAE) results in craniofacial defects in the absence of a diagnosis of FAS (7,8). Multiple factors contribute to the impact of PAE, in particular genetic predisposition (5). To date, several ethanol-sensitizing alleles in zebrafish, mouse and humans have been linked with increased cell death, holoprosencephaly, oral clefting, disruption to axonal projections, and broad neural and eye defects (9–13). Despite these growing insights into the genetic components contributing to risk for FASD, we lack mechanistic insights into ethanol-sensitive gene function and associated cellular mechanisms during development that underlie FASD (5).

Increasing evidence from several vertebrates including humans shows that genetic factors modulate developmental ethanol sensitivity (5). Studying FASD in humans remains challenging due to the complex interplay of genetic background with often incompletely documented ethanol timing and dosage. Genetically tractable model organisms, such as zebrafish, have been essential in improving our understanding of the genetic loci behind the variability in FASD (14). The zebrafish is well-suited for studying ethanol-sensitizing genetics because of its genetic tractability, high fecundity, external fertilization, embryo transparency, and rapid development (11,12,15). We have previously used both a candidate-based and an un-biased forward-genetic screen-based approach to identify ethanol-sensitive mutations (11,12,15) and these approaches have proven successful in predicting human gene-ethanol interactions (11). However, despite the increasing number of identified ethanol-sensitive loci, we lack a conceptual and mechanistic understanding of how these gene-ethanol interactions affect the diverse cell types and cellular behaviors underlying craniofacial development.

Previous work has established that both the genetic pathways required in, and the cellular events for, development of the craniofacial skeleton are deeply conserved between zebrafish and mammals (16–18). Cranial neural crest cells (CNCC) give rise to the majority of the craniofacial skeleton and migrate from the dorsal neural tube to populate progenitor structures called the pharyngeal arches (16–18). Concurrent with cranial neural crest cell migration, the pharyngeal endoderm undergoes its own cellular rearrangements and tissue movements to form a midline epithelial sheet with lateral protrusions called "pouches". Proper morphogenesis of the pharyngeal endoderm is critical for craniofacial development, in particular of the jaw (19–24). Work in zebrafish has shown that several genetic pathways regulate endodermal morphogenesis (19,21,24–28). One such pathway is the Bone Morphogenetic Protein (Bmp) signaling pathway. Comprised of over 60 pathway components with different spatio-temporal expression and activity, active Bmp signaling initiates with heterodimer ligands binding to a complex of two type I and two type II transmembrane receptors that regulate downstream target genes through phosphorylation of Smad proteins (29,30). Two major interacting ligands of the pathway are Bmp2b and Bmp4, both of which have a higher binding affinity type I Bmp receptors, such as Bmpr1bb over type II receptors (30,31). We have previously shown that Bmp signaling is required in the endoderm to regulate a Fibroblast Growth Factor (Fgf) signaling response in the forming pouches (24). Chemical inhibition of BMP signaling impairs the morphogenesis of both pouches and the anterior pharyngeal endoderm as the area of endoderm anterior to the first pouch, resulting in craniofacial malformations (24). These observations showed that functional Bmp signaling is indispensable for establishing proper endoderm morphology as necessary for uninterrupted craniofacial skeleton patterning.

As a complex pathway that is essential for craniofacial morphogenesis, we hypothesized that BMP signaling is potentially ethanol-sensitive. Here, we tested the ethanol sensitivity mutations in several components of the Bmp pathway in zebrafish. We show that hemi- or homozygous mutants for the Bmp ligand genes *bmp2b* and *bmp4* and for the receptor gene *bmpr1bb* (defined as Bmp mutants henceforth) predispose zebrafish embryos to distinct ethanol-induced craniofacial shape changes, particularly jaw malformations. Using quantitative morphometrics, we show that ethanol-induced disruptions to anterior pharyngeal endoderm shape, which mirror changes in facial shapes, alter the expression domain of the oral ectoderm

marker *fgf8a* as associated with jaw malformations. Genetic analysis shows that *BMPR1B* associates with jaw deformations in children with ethanol exposure that mirror our zebrafish data, underlining the predictive strength of our zebrafish findings. Collectively, our data links perturbations in Bmp signaling to ethanol susceptibility during craniofacial development in zebrafish and humans, establishing mechanistic concepts in gene-ethanol interactions for future studies in FASD.

## Results

### Mutations in multiple components of the Bmp pathway sensitize embryos to ethanol-induced viscerocranial malformations

Our previous work showed that Bmp signaling in zebrafish is required for pharyngeal endoderm patterning from 10-18 hpf (24). We therefore hypothesized that mutations in Bmp signaling pathway components would sensitize larvae to ethanol-induced craniofacial malformations. The Bmp ligand genes *bmp2b* and *bmp4* are expressed adjacent to the development endoderm during this time window, making mutants for these genes ideal targets for ethanol-sensitivity testing (24). Both of Bmp2b and Bmp4 have a higher binding affinity type I Bmp receptors over type II (30,31); as such, we also tested the receptor mutant *bmpr1bb* (32) for ethanol sensitivity.

To test these Bmp signaling mutants, we exposed embryos to a sub-phenotypic dose of 1% ethanol (v/v) from 10-18 hpf, the same window when Bmp signaling is required for endoderm morphogenesis and jaw development (24). We selected 1% ethanol (v/v) as the highest dose that does not cause craniofacial defects in wild type embryos, while higher doses of 1.25% and up have been shown to impact facial development (11,12,33–35). 1% ethanol (v/v) equilibrates within 5 minutes of exposure to an average ethanol tissue concentration of 50 mM (approximately 30% of the media) (13,36–38). Importantly, this embryonic ethanol concentration is roughly equivalent to a human BAC of 0.23; while a binge dose, is physiologically relevant to FASD and humans are readily capable of surpassing this amount (39–43).

Using this exposure paradigm, we found that mutations in our chosen Bmp mutants sensitize developing zebrafish to a range of ethanol-induced developmental defects, including small eyes and, for this work, jaw malformations (Fig. 1A-H). While *bmp2b*$^{-/-}$ embryos do not develop past 16 hpf (44), heterozygous *bmp2b*$^{+/-}$

, *bmp4*$^{-/-}$, or *bmpr1bb*$^{-/-}$ larvae undergo normal craniofacial development and are superficially indistinguishable from their wild type siblings (Fig. 1A-D). However, when exposed to ethanol using our conditions of 1% ethanol (v/v), these Bmp mutants developed a variable range of jaw defects from malformations to outright absence of the jaw (Fig. 1 E-F).

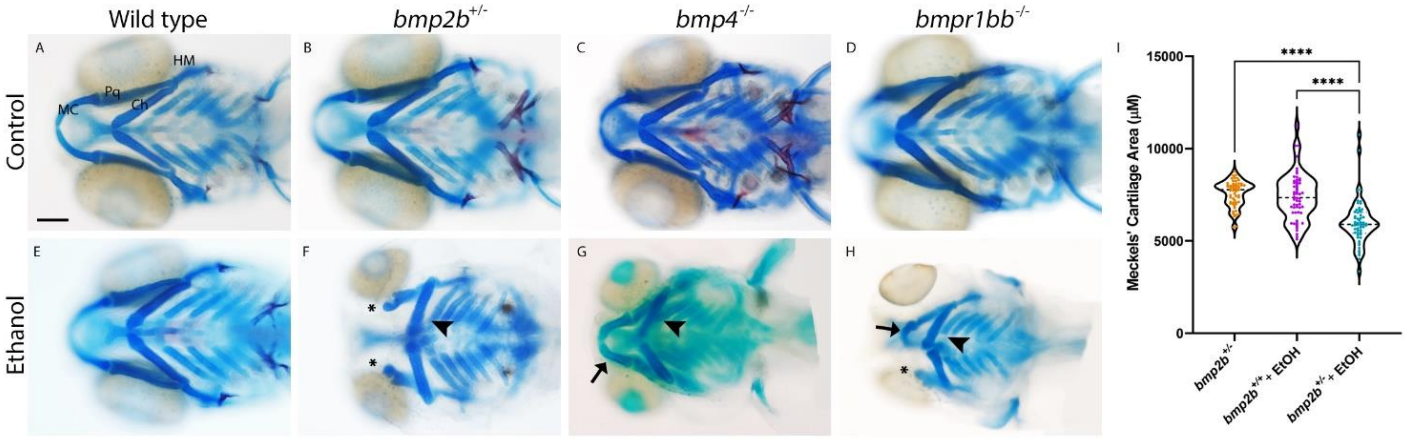


**Figure 1. Multiple members of the Bmp pathway display ethanol sensitive facial phenotypes.** (**A-H**) Whole-mount images of viscerocranium at 5 dpf larva. Cartilage is blue and bone is red (Ventral views, anterior to the left, scale bar: 100 µm, MC = Meckel's, Pq = palatoquadrate, Ch = ceratohyal and HM = hyomandibular cartilages). (**I**) Area measures of the Meckel's cartilage. (**A-D**) *bmp2b*$^{+/-}$ or *bmp4*$^{-/-}$ or *bmpr1bb*$^{-/-}$ larva develop comparable to Wild type larva. (**E-H**) Exposure of 1% ethanol exposure from 10-18 hpf results in a range of defects to the viscerocranium, from loss of MC (asterisks) to reductions in size and changes in shape in the MC (arrows) as well as a flattening of the Ch (arrowheads) in the Bmp mutant alleles but not in Wild type siblings. (**I**) The size Meckel's cartilage element was reduced in ethanol-treated *bmp2b*$^{+/-}$ larva compared to ethanol-treated *bmp2b*$^{+/+}$ and untreated *bmp2b*$^{+/-}$ larva (F=36.85, p=.0001, one-way ANOVA, n=58 cartilage elements per group).

Jaw malformations were more common in ethanol-treated Bmp mutants than absent jaw, with 15.9% vs 4.6% in *bmp2b*$^{+/-}$, 37.8% vs 6.13% in *bmp4*$^{-/-}$, and 29.1% vs 2.7% in *bmpr1bb*$^{-/-}$, with variation between experimental groups (Table 1). Our quantifications also demonstrated that while wild type siblings never displayed sensitivity to ethanol, heterozygous *bmp4*$^{+/-}$ and *bmpr1bb*$^{+/-}$ larva were ethanol sensitive with incomplete penetrance (Table 1). These results reveal that viscerocranial malformations, in particular jaw absence, occur in ethanol-treated zebrafish with Bmp pathway mutations but not in either Bmp mutant or ethanol treatment alone.

**Ethanol alters overall shape of the viscerocranium in Bmp mutants**

Micrognathia is a hallmark of ethanol exposure in humans, though recent data has shown greater variation in facial shape in FASD (6,7). To understand the impact of ethanol on viscerocranial shape and size, we undertook as series of quantitative measures to directly assess facial shape changes in zebrafish. To

**Table 1. Gene-ethanol penetrance**

| Experiments | Untreated Embryos | EtOH-treated Embryos | Jaw Malformations | Percent | Jaw Loss | Percent |
|---|---|---|---|---|---|---|
| | | | ***bmp2b*** | | | |
| 1 | 37 | 41 | 6 | 14.6% | 0 | 0.0% |
| 2 | 45 | 41 | 10 | 24.4% | 3 | 7.3% |
| 3 | 37 | 115 | 20 | 17.4% | 4 | 3.5% |
| 4 | 80 | 46 | 9 | 19.6% | 5 | 10.9% |
| 5 | 64 | 61 | 12 | 19.7% | 1 | 1.6% |
| 6 | 75 | 193 | 26 | 13.5% | 7 | 3.6% |
| 7 | 23 | 24 | 0 | 0.0% | 4 | 16.7% |
| Totals | 361 | 521 | 83 | 15.9% | 24 | 4.6% |
| | | | ***bmp4*** | | | |
| 1 | 24 | 63 | 30 | 47.6% | 3 | 4.8% |
| 2 | 41 | 131 | 38 | 29.0% | 2 | 1.5% |
| 3 | 42 | 38 | 24 | 63.2% | 2 | 5.3% |
| 4 | 51 | 94 | 20 | 21.3% | 16 | 17.0% |
| 5 | 44 | 82 | 42 | 51.2% | 2 | 2.4% |
| Totals | 202 | 408 | 154 | 37.7% | 25 | 6.1% |
| | | | ***bmpr1bb*** | | | |
| 1 | 105 | 82 | 41 | 50.0% | 1 | 1.2% |
| 2 | 48 | 38 | 1 | 2.6% | 0 | 0.0% |
| 3 | 154 | 69 | 13 | 18.8% | 4 | 5.8% |
| Totals | 307 | 189 | 55 | 29.1% | 5 | 2.6% |

**Table 1. Penetrance of gene-ethanol interactions in Bmp mutants.** Percent of jaw malformations and jaw loss per experiment in ethanol-treated Bmp single mutants.

quantify micrognathia-like reductions in jaw size observed in FASD, we dissected and measured the size of the Meckel's cartilages from untreated *bmp2b*$^{+/-}$ and ethanol-treated *bmp2b*$^{+/+}$ and *bmp2b*$^{+/-}$ larvae. Ethanol-treated *bmp2b*$^{+/-}$ larvae displayed a significant reduction in jaw size compared to untreated *bmp2b*$^{+/-}$ and ethanol-treated *bmp2b*$^{+/+}$ larvae (Fig. 1I, one-way ANOVA, $F=36.85$, $p<.0001$). Beyond jaw defects, we observed malformations in additional viscerocranial cartilage elements, in particular an increase of the angle between the ceratohyal (Ch) elements (Fig. 1B-D compared to F-H). To expand our assessment of Bmp-ethanol interactions on facial shape, we performed morphometric analysis on untreated and ethanol-treated *bmp4*$^{+/+}$ and *bmp4*$^{-/-}$ larvae. We analyzed *bmp4* larvae as they showed the greatest variation due to ethanol treatment. (Table 1). We determined facial shape by labeling each joint in the viscerocranium (Fig. 2A, Alcian Blue-stained image). Principle component analysis (PCA) of facial shape revealed that PC1 represented over 50% of facial variation as a shortening and widening of the viscerocranium, as well as a flattening of the angles of several cartilage elements (Fig. 2A, Principal component 1). PC2 represented nearly 20% of the variation in facial shape, affecting width of the midface (Fig. 2A, Principal component 2).

Our dataset shows that the greatest amount of variation occurred in ethanol-treated *bmp4*$^{-/-}$ larvae, while the smallest variation occurred in wild type, *bmp4*$^{+/+}$ larvae (Fig. 2A, magenta dashed vs black dashed 95% confidence ellipses). Ethanol-treated *bmp4*$^{+/+}$ and untreated *bmp4*$^{-/-}$ larvae displayed similar increases in variation compared to untreated *bmp4*$^{+/+}$ larvae, but less than ethanol-treated *bmp4*$^{-/-}$ larvae. The mean of each group, displayed as a solid ellipse centered in the 95% confidence ellipse, shows little overlap between the groups (Fig. 2A). Procrustes ANOVA analysis showed that these shape changes were significant ($F=10.37$, $p<.0001$). Combined, our morphometric data set shows that ethanol-treated *bmp4*$^{-/-}$ larvae displayed significant variation in facial shape; however, either ethanol or *bmp4*$^{-/-}$ alone also increased variation in viscerocranial shape compared to untreated *bmp4*$^{+/+}$ larvae. We did not identify this variation in ethanol or *bmp4*$^{-/-}$ alone in our initial visual screens. Overall, this data shows that ethanol-treated Bmp mutant larvae have significant, quantifiable changes in facial size and shape compared that are not readily identified in visual screens for gross morphology.

To confirm the morphometric data, we performed linear measurements on the viscerocrania of the *bmp4* morphometric dataset. We measured the length between the midline joints of the Meckel's and ceratohyal cartilages and the width between the joints of the Meckel's and palatoquadrate cartilages and ceratohyal and palatoquadrate cartilages (Fig. 2B). We further performed angle measures of the joints of the Meckel's and ceratohyal cartilages to analyze the flattening of the viscerocranium cartilage elements (Fig. 2F). Consistent with PC1 (Fig. 2A), we observed a significant decrease in the length between the Meckel's and ceratohyal cartilages in ethanol-treated *bmp4*$^{-/-}$ larvae compared to all other groups (Fig. 2C, Table 2). We observed significant changes in facial width at both the Meckel's and palatoquadrate cartilages and ceratohyal and palatoquadrate cartilages (Fig. 2D and E, respectively, Table 2). In both measures, ethanol-treated *bmp4*$^{-/-}$ larva showed significant decreases in width at both the Meckel's and palatoquadrate cartilages and ceratohyal and palatoquadrate cartilages compared to untreated *bmp4*$^{+/+}$ larvae and untreated *bmp4*$^{-/-}$ larva (Fig. 2D-E, Table 2). In contrast, untreated *bmp4*$^{-/-}$ larvae showed an increase in viscerocranial width compared to all other groups; the measurements were significantly increased compared to ethanol-treated *bmp4*$^{+/+}$ and *bmp4*$^{-/-}$ larvae (Fig. 2D-E, Table 2) and trending toward significance compared to untreated wild type embryos in Fig. 2D (Table 2) but not in Fig. 2E (Table 2). In angle measures of the Meckel's and ceratohyal cartilages, ethanol-treated *bmp4*$^{-/-}$ larvae showed significant increases in cartilage angles (Fig.

2G-H, Table 2), consistent with the flattening of the viscerocranial cartilages observed initial screens (Fig. 1)

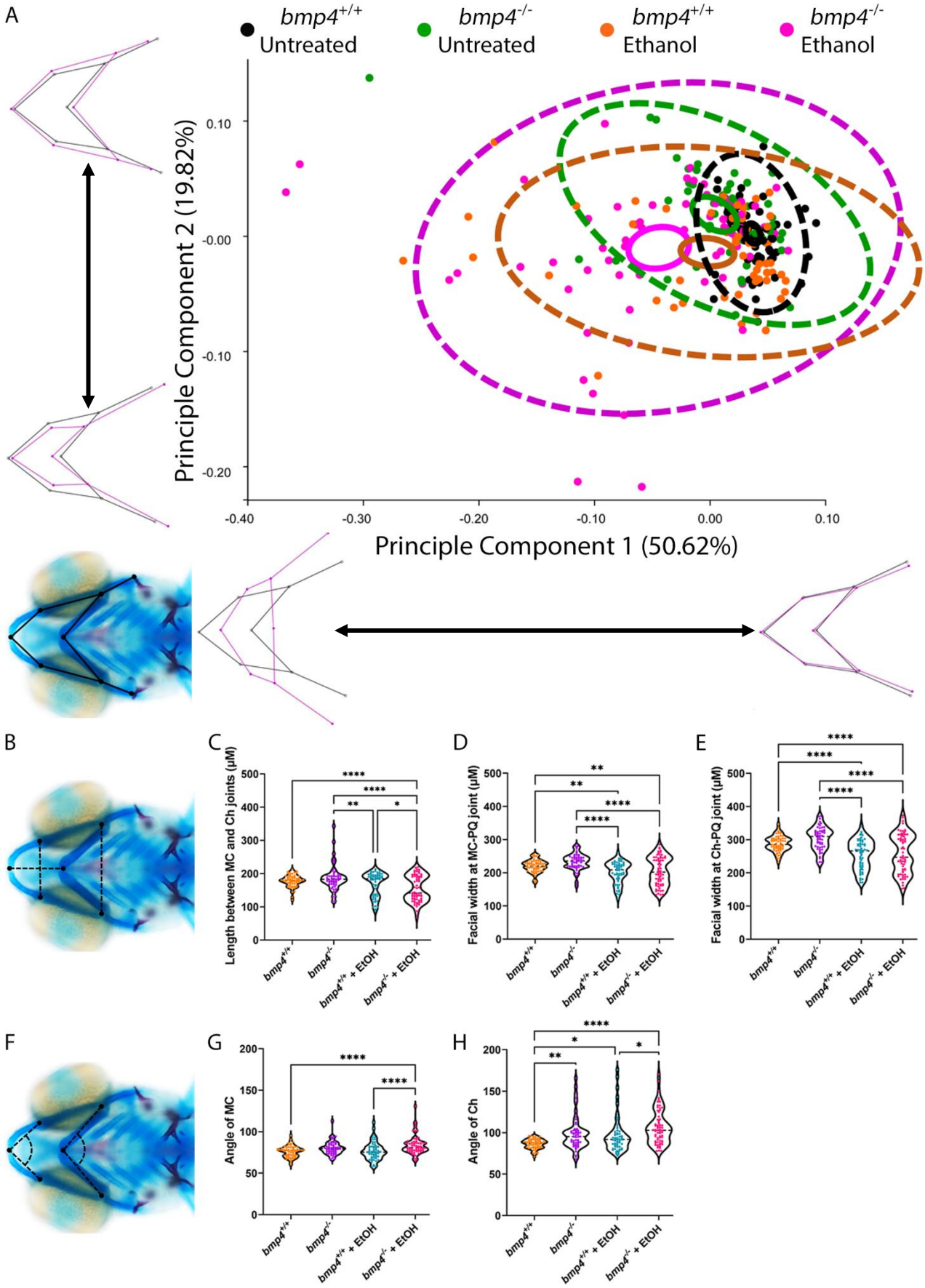


also

**Figure 2. Ethanol exposure alters viscerocranial shape in *bmp4*$^{-/-}$ larvae.** (**A, B, F**) Whole-mount images of the viscerocranium in 5 dpf larvae showing landmarks, linear measures and cartilage angles (cartilage is blue and bone is red, ventral views, anterior to the left). (**A**) Landmarks were placed on several joints between the cartilage elements of the viscerocranium. Genotypes are color-coded; black = untreated *bmp4*$^{+/+}$ larvae (n = 61), green = untreated *bmp4*$^{-/-}$ larvae (n = 54), orange = ethanol-treated *bmp4*$^{+/+}$ larvae (n = 58), magenta = ethanol-treated *bmp4*$^{-/-}$ larvae (n = 66), dashed circles represent confidence ellipses in

which 95% of all individual data points for each group lie, solid circles represent 95% confidence ellipses for means. Wireframe graphs represent variation described by each axis with black representing no variation and magenta representing variation relative to the black wireframe. For example, PC1 captures a shortening and widening in viscerocranial shape, while PC2 represents variation in midfacial width. Procrustes ANOVA showed significant change in the viscerocranial shape (F = 10.37, DF = 36, p = .0001). (**C**) Length measures between the midline joints of the Meckel's cartilages and ceratohyal cartilages and width measures between the joints of the (**D**) Meckel's and palatoquadrate cartilages and (**E)** ceratohyal and palatoquadrate cartilages. Measures of angles joint of the (**G**) Meckel's and (**H**) ceratohyal cartilages. Linear measures show significant decrease in facial width and length and an increase in angle between cartilage elements, representing flattening of the facial skeleton (Individual graph statistics in Table 2).

**Table 2. Linear Measure Statistics for Figure 2**

| **Length at MC-Ch joints** | | | **Width at MC/PQ joint** | | | **Width at Ch-PQ joint** | | |
|---|---|---|---|---|---|---|---|---|
| **ANOVA** | F = 14.94 | P < 0.0001 | **ANOVA** | F = 15.62 | P < 0.0001 | **ANOVA** | F = 23.77 | P < 0.0001 |
| **Tukey's Comparisons** | | | **Tukey's Comparisons** | | | **Tukey's Comparisons** | | |
| *bmp4*$^{+/+}$ vs *bmp4*$^{-/-}$ | p = 0.3411 | | *bmp4*$^{+/+}$ vs *bmp4*$^{-/-}$ | p = 0.0508 | | *bmp4*$^{+/+}$ vs *bmp4*$^{-/-}$ | p = 0.0858 | |
| *bmp4*$^{+/+}$ vs *bmp4*$^{+/+}$ + EtOH | p = 0.3296 | | *bmp4*$^{+/+}$ vs *bmp4*$^{+/+}$ + EtOH | p = 0.0055 | | *bmp4*$^{+/+}$ vs *bmp4*$^{+/+}$ + EtOH | p < 0.0001 | |
| *bmp4*$^{+/+}$ vs *bmp4*$^{-/-}$ + EtOH | p < 0.0001 | | *bmp4*$^{+/+}$ vs *bmp4*$^{-/-}$ + EtOH | p = 0.0082 | | *bmp4*$^{+/+}$ vs *bmp4*$^{-/-}$ + EtOH | p < 0.0002 | |
| *bmp4*$^{-/-}$ vs *bmp4*$^{+/+}$ + EtOH | p = 0.006 | | *bmp4*$^{-/-}$ vs *bmp4*$^{+/+}$ + EtOH | p < 0.0001 | | *bmp4*$^{-/-}$ vs *bmp4*$^{+/+}$ + EtOH | p < 0.0003 | |
| *bmp4*$^{-/-}$ vs *bmp4*$^{-/-}$ + EtOH | p < 0.0001 | | *bmp4*$^{-/-}$ vs *bmp4*$^{-/-}$ + EtOH | p < 0.0001 | | *bmp4*$^{-/-}$ vs *bmp4*$^{-/-}$ + EtOH | p < 0.0004 | |
| *bmp4*$^{+/+}$ + EtOH vs *bmp4*$^{-/-}$ + EtOH | p = 0.0144 | | *bmp4*$^{+/+}$ + EtOH vs *bmp4*$^{-/-}$ + EtOH | p = 0.997 | | *bmp4*$^{+/+}$ + EtOH vs *bmp4*$^{-/-}$ + EtOH | p = 0.9993 | |
| **Angle at MC** | | | **Angle at Ch** | | | | | |
| **ANOVA** | F = 10.01 | P < 0.0001 | **ANOVA** | F = 12.33 | P < 0.0001 | | | |
| **Tukey's Comparisons** | | | **Tukey's Comparisons** | | | | | |
| *bmp4*$^{+/+}$ vs *bmp4*$^{-/-}$ | p = 0.0653 | | *bmp4*$^{+/+}$ vs *bmp4*$^{-/-}$ | p = 0.0015 | | | | |
| *bmp4*$^{+/+}$ vs *bmp4*$^{+/+}$ + EtOH | p = 0.9995 | | *bmp4*$^{+/+}$ vs *bmp4*$^{+/+}$ + EtOH | p = 0.0192 | | | | |
| *bmp4*$^{+/+}$ vs *bmp4*$^{-/-}$ + EtOH | p < 0.0001 | | *bmp4*$^{+/+}$ vs *bmp4*$^{-/-}$ + EtOH | p < 0.0001 | | | | |
| *bmp4*$^{-/-}$ vs *bmp4*$^{+/+}$ + EtOH | p = 0.0866 | | *bmp4*$^{-/-}$ vs *bmp4*$^{+/+}$ + EtOH | p = 0.8338 | | | | |
| *bmp4*$^{-/-}$ vs *bmp4*$^{-/-}$ + EtOH | p = 0.1873 | | *bmp4*$^{-/-}$ vs *bmp4*$^{-/-}$ + EtOH | p = 0.1914 | | | | |
| *bmp4*$^{+/+}$ + EtOH vs *bmp4*$^{-/-}$ + EtOH | p < 0.0001 | | *bmp4*$^{+/+}$ + EtOH vs *bmp4*$^{-/-}$ + EtOH | p = 0.0204 | | | | |

**Table 2. Statistical analyses of linear facial measures in Figure 2.** Alcian/alizarin-stained viscerocraniums were analyzed with a two-way ANOVA (type III). F-statistic and P-value for each analysis are shown. A Tukey's Multiple Comparisons Test for each comparison are shown.

and PC1 and PC2 of our morphometric analysis (Fig. 2A). Overall, our morphometric measurements document that the Bmp-ethanol interaction results in a smaller jaw, and shorter and wider viscerocranial shape, consistent with FASD in humans (7,45).

**Combinatorial loss of Bmp pathway components exacerbates ethanol-induced viscerocranial malformations**

While we consistently observed ethanol-induced viscerocranial shape changes in tested Bmp mutants that differed from wild type controls, both the penetrance and expressivity of these defects were highly variable (Figs. 1-2, Table 1). The Bmp pathway is a complex signaling pathway comprised of multiple components (30). These components can be partially redundant at different levels of the pathway (46–49). Given this redundancy, we hypothesized that combinatorial loss of pathway components potentially increases both the penetrance and expressivity of ethanol-induced viscerocranial defects. Using a hypomorphic *smad5* allele that has a highly stereotyped phenotype of cartilage fusions and malformations and have been previously shown to be insensitive to ethanol exposure (11,50), we generated double-mutant *bmp4*$^{-/-}$;*smad5*$^{-/-}$ larvae (Fig. 3). We found that *bmp4*$^{-/-}$;*smad5*$^{-/-}$ larvae exhibit 100% penetrant, ethanol-induced viscerocranial

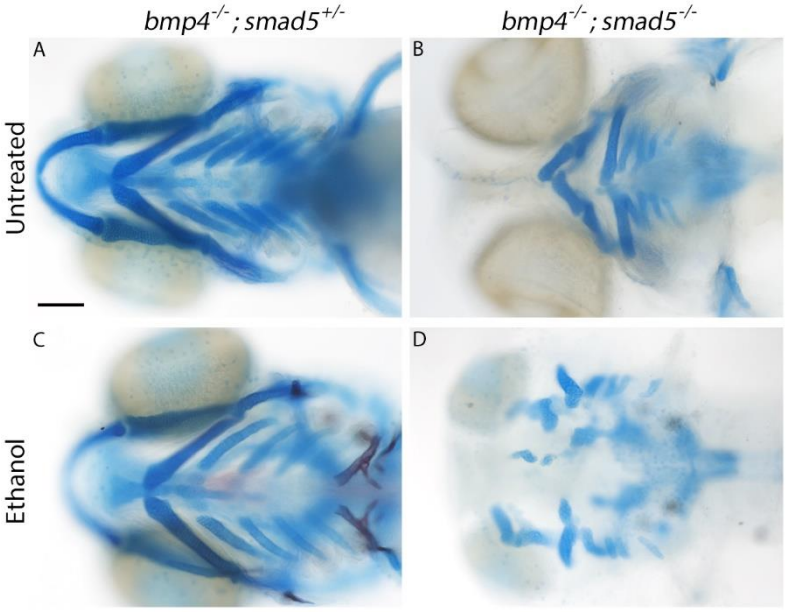


**Figure 3. Ethanol exposure alters area of the anterior pharyngeal endoderm in *bmp4*$^{-/-}$;*smad5*$^{-/-}$ larvae.** (**A-D**) Whole-mount images of viscerocranium at 5 dpf larvae. Cartilage is blue and bone is red (Ventral views, anterior to the left, scale bar: 100 µm). (**A**) No impact on facial formation was observed in untreated *bmp4*$^{-/-}$;*smad5*$^{+/-}$ larvae. (**B**) Stereotypical *smad5* mutant phenotypes were observed in *bmp4*$^{-/-}$;*smad5*$^{-/-}$ larvae. (**C**) Ethanol does not impact viscerocranial morphology in *bmp4*$^{-/-}$;*smad5*$^{+/-}$ larvae. (**D**) However, *bmp4*$^{-/-}$;*smad5*$^{-/-}$ larvae are fully penetrant, ethanol sensitive, resulting several viscerocranial malformations recapitulating the severe phenotypes in Dorsomorphin-treated embryos (24).

malformations that are a) more severe than the stereotypical *smad5* phenotypes in untreated *bmp4*$^{-/-}$;*smad5*$^{-/-}$ larvae and b) much more severe than any of the Bmp single mutants (Fig. 3D compared to B; compared to Fig. 1). We also observed a spectrum of phenotype severity in *bmp4*$^{+/-}$;*smad5*$^{-/-}$ larvae, in which one gene copy of *bmp4* remained wild-type: these phenotypes range from stereotypical *smad5* mutant phenotypes to phenotypes comparable to ethanol-treated double-homozygous *bmp4*$^{-/-}$;*smad5*$^{-/-}$ larvae (Supp. Fig. 2). In contrast, we observed no impact of ethanol on double-heterozygous *bmp4*$^{+/-}$;*smad5*$^{+/-}$ larvae (data not shown). These genetic interaction results indicate that the variation in *bmp*$^{+/-}$;*smad5*$^{-/-}$ larvae may be driven either by expression differences in other components of the Bmp pathway or additional yet identified

ethanol-sensitive alleles. Ultimately, these data supports our previous observation in *bmp4*$^{-/-}$ larvae that ethanol-induced phenotypes only occur in the combination of mutation and ethanol exposure, indicating that the interaction of Bmp signaling with ethanol is synergistic during craniofacial development.

**Ethanol-treated Bmp mutants display malformations to the anterior pharyngeal endoderm and *fgf8a* expression in the oral ectoderm**

We have previously shown that zebrafish embryos treated with the Bmp signaling inhibitor compound Dorsomorphin from 10-18 hpf exhibit disrupted morphogenesis of the anterior pharyngeal endoderm (24). Multiple studies have shown that disruptions to the anterior pharyngeal endoderm leads to jaw malformations (19–23). To analyze anterior pharyngeal endoderm shape, we labeled the pharyngeal endoderm by crossing the *sox17:EGFP* transgene, which labels all endoderm with EGFP (51), into the *bmp4*$^{-/-}$*;smad5*$^{-/-}$ background. Compared to wild type, ethanol-treated *bmp4*$^{-/-}$*;smad5*$^{-/-}$ embryos showed mild changes to overall endoderm shape (Fig. 4A-D). However, our more detailed examination showed that the

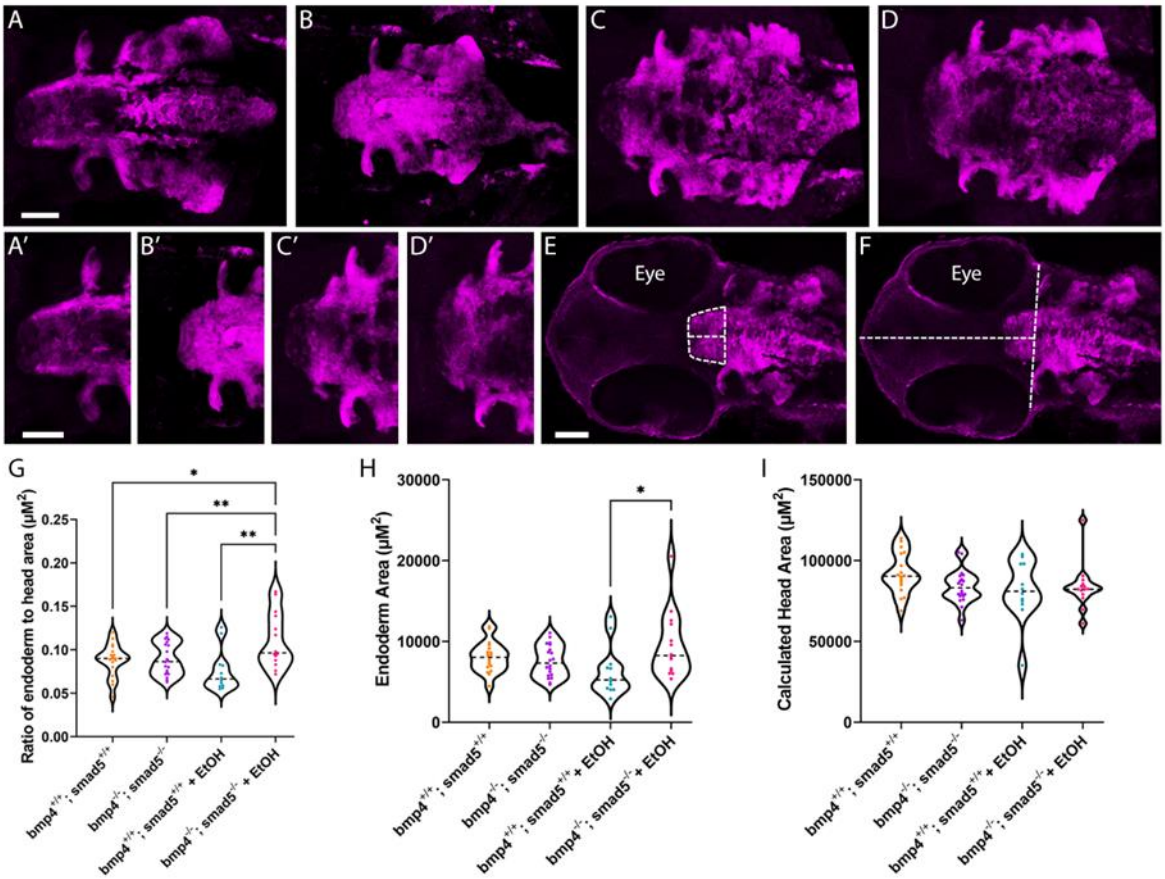


**Figure 4. Ethanol exposure alters area of the anterior pharyngeal endoderm in *bmp4*$^{-/-}$*;smad5*$^{-/-}$ embryos.** (**A-D**) Whole-mount images of pharyngeal endoderm in 36 hpf embryos; (**A'-D'**) magnified view of the anterior pharyngeal endoderm (untreated *bmp4*$^{+/+}$*;smad5*$^{+/+}$ embryos, n = 18, **A, A'**; untreated *bmp4*$^{-/-}$*;smad5*$^{-/-}$ embryos, n = 20, **B, B'**; ethanol-treated *bmp4*$^{+/+}$*;smad5*$^{+/+}$ embryos, n = 12, **C, C'**; ethanol-treated *bmp4*$^{-/-}$*;smad5*$^{-/-}$ embryos, n = 14, **D, D'**; dorsal views, anterior to the left; Size bars: 50 μm). (**E**) Area and length of the anterior pharyngeal endoderm was measured from the first pouch to the anterior-most tip while width of the anterior pharyngeal endoderm was measured at the level of the first pouch. (**F**) Area of the head

was calculated from length (first pouch to most anterior tip of the head) and width (measured at the level of the first pouch) of the head. (**G**) Ratio of anterior pharyngeal endoderm to head area shows that ethanol-treated *bmp4*$^{-/-}$;*smad5*$^{-/-}$ embryos show increased area of the anterior endoderm compared to all other groups. This increased size is not due to changes in head size (**H**) but due to increased size in the anterior pharyngeal endoderm directly (I, individual graph statistics in Table 3).

shape of the anterior pharyngeal endoderm is altered in ethanol-treated *bmp4*$^{-/-}$;*smad5*$^{-/-}$ embryos (Fig. 4A'-D'). To quantify these changes in anterior pharyngeal endoderm shape, we measured width at the first pouch (AE width), midline length (AE length) and area anterior pharyngeal endoderm (AE area) from the first pouch to the anterior most end of the pharyngeal endoderm (Fig. 4E). We normalized for ethanol-induced general growth deficits to anterior pharyngeal endoderm shape, by measuring the length and width of the embryonic head and calculating head area (Fig. 4F). Calculating head area controls for ethanol-induced reductions in eye size and did not show any differences between groups (Fig. 4I). Our analyses showed a significant increase in AE area expressed as a ratio to head area in ethanol-treated double-homozygous *bmp4*$^{-/-}$;*smad5*$^{-/-}$ embryos compared to all other groups (Fig. 4G, Table 3). AE area alone of ethanol-treated *bmp4*$^{-/-}$;*smad5*$^{-/-}$ embryos only exhibited a significant increase compared to ethanol-treated wild type, *bmp4*$^{+/+}$;*smad5*$^{+/+}$ embryos (Fig. 4H, Table 3). We also observed trends in linear measures with ethanol-

**Table 3. Statistics for Figure 4**

| Ratio of Endoderm to Head Area | | Endoderm Area | | Head Area (Calculated) | |
|---|---|---|---|---|---|
| **ANOVA** | F = 5.919 P = 0.0019 | **ANOVA** | F = 2.801 P = 0.0518 | **ANOVA** | F = 1.958 P = 0.1353 |
| **Tukey's Comparisons** | | **Tukey's Comparisons** | | **Tukey's Comparisons** | |
| *bmp4*$^{+/+}$;*smad5*$^{+/+}$ vs *bmp4*$^{-/-}$;*smad5*$^{+/+}$ | p = 0.9989 | *bmp4*$^{+/+}$;*smad5*$^{+/+}$ vs *bmp4*$^{-/-}$;*smad5*$^{+/+}$ | p = 0.8751 | *bmp4*$^{+/+}$;*smad5*$^{+/+}$ vs *bmp4*$^{-/-}$;*smad5*$^{+/+}$ | p = 0.3505 |
| *bmp4*$^{+/+}$;*smad5*$^{+/+}$ vs *bmp4*$^{+/+}$;*smad5*$^{+/+}$ + EtOH | p = 0.8727 | *bmp4*$^{+/+}$;*smad5*$^{+/+}$ vs *bmp4*$^{+/+}$;*smad5*$^{+/+}$ + EtOH | p = 0.8751 | *bmp4*$^{+/+}$;*smad5*$^{+/+}$ vs *bmp4*$^{+/+}$;*smad5*$^{+/+}$ + EtOH | p = 0.1492 |
| *bmp4*$^{+/+}$;*smad5*$^{+/+}$ vs *bmp4*$^{-/-}$;*smad5*$^{-/-}$ + EtOH | p = 0.0127 | *bmp4*$^{+/+}$;*smad5*$^{+/+}$ vs *bmp4*$^{-/-}$;*smad5*$^{-/-}$ + EtOH | p = 0.8751 | *bmp4*$^{+/+}$;*smad5*$^{+/+}$ vs *bmp4*$^{-/-}$;*smad5*$^{-/-}$ + EtOH | p = 0.2876 |
| *bmp4*$^{-/-}$;*smad5*$^{-/-}$ vs *bmp4*$^{+/+}$;*smad5*$^{+/+}$ + EtOH | p = 0.9211 | *bmp4*$^{-/-}$;*smad5*$^{-/-}$ vs *bmp4*$^{+/+}$;*smad5*$^{+/+}$ + EtOH | p = 0.8751 | *bmp4*$^{-/-}$;*smad5*$^{-/-}$ vs *bmp4*$^{+/+}$;*smad5*$^{+/+}$ + EtOH | p = 0.8835 |
| *bmp4*$^{-/-}$;*smad5*$^{-/-}$ vs *bmp4*$^{-/-}$;*smad5*$^{-/-}$ + EtOH | p = 0.0089 | *bmp4*$^{-/-}$;*smad5*$^{-/-}$ vs *bmp4*$^{-/-}$;*smad5*$^{-/-}$ + EtOH | p = 0.1277 | *bmp4*$^{-/-}$;*smad5*$^{-/-}$ vs *bmp4*$^{-/-}$;*smad5*$^{-/-}$ + EtOH | p = 0.992 |
| *bmp4*$^{-/-}$;*smad5*$^{-/-}$ + EtOH vs *bmp4*$^{-/-}$;*smad5*$^{-/-}$ + EtOH | p = 0.0033 | *bmp4*$^{-/-}$;*smad5*$^{-/-}$ + EtOH vs *bmp4*$^{-/-}$;*smad5*$^{-/-}$ + EtOH | p = 0.0494 | *bmp4*$^{-/-}$;*smad5*$^{-/-}$ + EtOH vs *bmp4*$^{-/-}$;*smad5*$^{-/-}$ + EtOH | p = 0.9686 |

**Table 3. Statistical analyses of endoderm/head area measures in Figure 4.** Measures of anterior endoderm/head area were analyzed with a two-way ANOVA (type III). F-statistic and P-value for each analysis are shown. A Tukey's Multiple Comparisons Test for each comparison are shown.

treated *bmp4*$^{-/-}$;*smad5*$^{-/-}$ embryos showing increases in AE length and AE width while no differences were observed in head length and width (Supp. Fig. 3, Supp. Table 1). Collectively, our observations in zebrafish

document that changes in anterior pharyngeal endoderm area in ethanol-treated Bmp mutants might underlie viscerocranial malformations.

Previous work has shown that the anterior pharyngeal endoderm is necessary to induce signaling factor expression in the oral ectoderm (19,22,23). This suggests that blocking Bmp signaling with either Dorsomorphin or ethanol will disrupt expression of the critical oral ectoderm markers, such as *fgf8a*. In wild type embryos, *fgf8a* is expressed in a small domain in the oral ectoderm, ventro-posterior to the developing eye and retina (Supp. Fig. 4A). Wild type embryos treated with Dorsomorphin from 10-18 hpf have variable defects in *fgf8a* expression with loss of expression being most common (Supp. Fig. 4B). This mirrors *fgf8a* expression changes in other anterior pharyngeal endoderm mutants (19,22). Interestingly, *pdgfaa* and *pdgfab* which are expressed throughout the oral ectoderm, are unaltered in Dorsomorphin-treated embryos (Supp. Fig. 4C-F), demonstrating that the oral ectoderm is not lost when Bmp signaling is attenuated and that the endoderm mediates the expression of some, but not all, oral ectodermal signaling molecules. To test if expression of *fgf8a* is altered in ethanol-treated *bmp4*$^{-/-}$;*smad5*$^{-/-}$ embryos, we performed HCR-based, fluorescent *in situ* hybridization. This expression domain of *fgf8a* was well-detectable in untreated *bmp4*$^{-/-}$;*smad5*$^{-/-}$ and ethanol-treated wild type, *bmp4*$^{+/+}$;*smad5*$^{+/+}$ embryos showing very little difference to untreated wild type embryos (Fig. 5A-C). Surprisingly, *fgf8a* expression in ethanol-treated *bmp4*$^{-/-}$;*smad5*$^{-/-}$ embryos was expanded anteriorly to the level of developing the retina (Fig. 5D). Our data of ethanol-

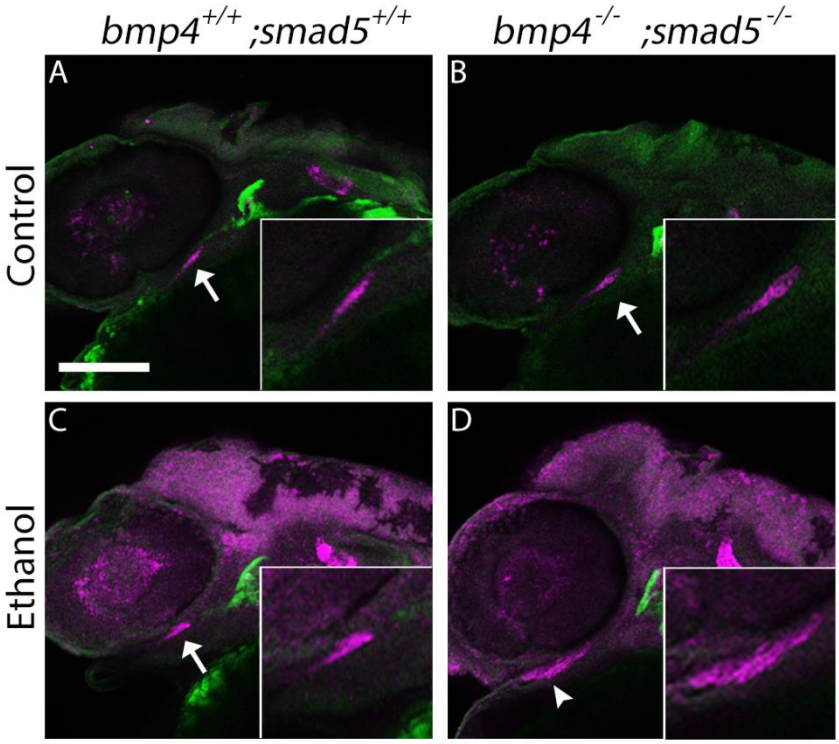

**Figure 5. Ethanol exposure changes shape of oral ectoderm expression domain in *bmp4*$^{-/-}$*;smad5*$^{-/-}$ embryos.** (**A-D**) Whole-mount, confocal images of *bmp4;smad5;sox17:EGFP* embryos fluorescently labeling *fgf8a* gene expression at 36 hpf (lateral views, anterior to the left, scale bar: 50 µm). (**A-C**) Arrows show normal expression of *fgf8a* in the oral ectoderm of untreated *bmp4*$^{+/+}$*;smad5*$^{+/+}$ and *bmp4*$^{-/-}$*;smad5*$^{-/-}$ embryos as well as ethanol-treated *bmp4*$^{+/+}$*;smad5*$^{+/+}$ embryos. (**D**) Arrowhead shows that domain of *fgf8a* expression in ethanol-treated *bmp4*$^{-/-}$*;smad5*$^{-/-}$ embryos is expanded anteriorly (n = 7 embryos per group).

induced changes upon Bmp signaling perturbation to the *fgf8a* expression domain in the oral ectoderm is consistent with previous work showing that malformations of the anterior pharyngeal endoderm disrupting oral ectoderm expression domains and subsequent viscerocranial malformations (19). While limited to *fgf8* as critical marker, these observations indicate that synergistic Bmp-ethanol perturbations disrupt an anterior pharyngeal endoderm-oral ectoderm-signaling axis.

**Bmp-ethanol interactions translate to human FASD jaw volume**

Zebrafish has been used successfully to model human developmental disorders (52,53) and we have previously shown that our zebrafish screens can predict gene-ethanol interactions in humans (11). We therefore sought to validate if our zebrafish model of Bmp-ethanol interactions impacting facial shape may be predictive of gene-ethanol associations in humans. From a study of children with and without PAE, we screened genome-wide association data for common variants in human *BMP2*, *BMP4*, and *BMPR1B* to explore if anomalous mandible volume was associated with a particular genotype in the presence or absence of PAE (genotype x PAE interaction). Only one SNP in the 5' region of *BMP2* (*rs235710*) was significant (p=0.029); no other SNPs in or near *BMP2* were correlated or demonstrated association (all p>0.74). Similarly, one SNP in the 5' region of *BMP4* (*rs72680543*, p=0.043) was significant but was in complete linkage disequilibrium (LD) (D'=1) with two SNPs that were non-significant (*rs72680541*, p=0.19; *rs10873077*, p=0.072). Given the lack of supporting evidence, we did not follow up on the findings in these two genes. The best p-value for SNPs in the BMP receptor gene *BMPR1B* was for *rs34063820* (p=4x10$^{-4}$, Minor Allele Frequency (MAF)=0.12; purple diamond in Fig. 6A). However, this result was not supported as there were no significant SNPs in strong LD with *rs34063820*. We therefore focused on a cluster of nine SNPs, which were in modest LD with *rs34063820* (r2<0.60). These SNPs also demonstrated association with mandible volume that differed according to PAE. The strongest genotype by PAE interaction in these nine SNPs was for *rs4397000* (purple diamond in Fig. 6B, p=0.016, all nine SNPs p<0.037). The *rs4397000* SNP had a minor allele (*A>C* allele) frequency of 0.209 in the European Ancestry (EA) sample and 0.496 in the African Ancestry (AA) sample. Eight of the nine SNPs are eQTLs, expressing *BMPR1B* in several

tissues. The minor allele *A* of *rs4397000* is associated with increased *BMPR1B* gene expression in the adrenal gland and decreased expression in the brain, heart, and pancreas. Wilcoxon test revealed that among children with an *AA* or *AC* genotype, there was no difference in mandible volume between the PAE (EA n=29, AA n=38) and no PAE (EA n=41, AA n=62; p=0.33) groups, though mandible volume was trending toward significance in the AA samples (EA p=0.70, AA p=0.052; all comparisons are shown in Fig. 6C). However, in EA individuals with two copies of the *C* allele, those without PAE (EA n=52, AA n=15; Fig.

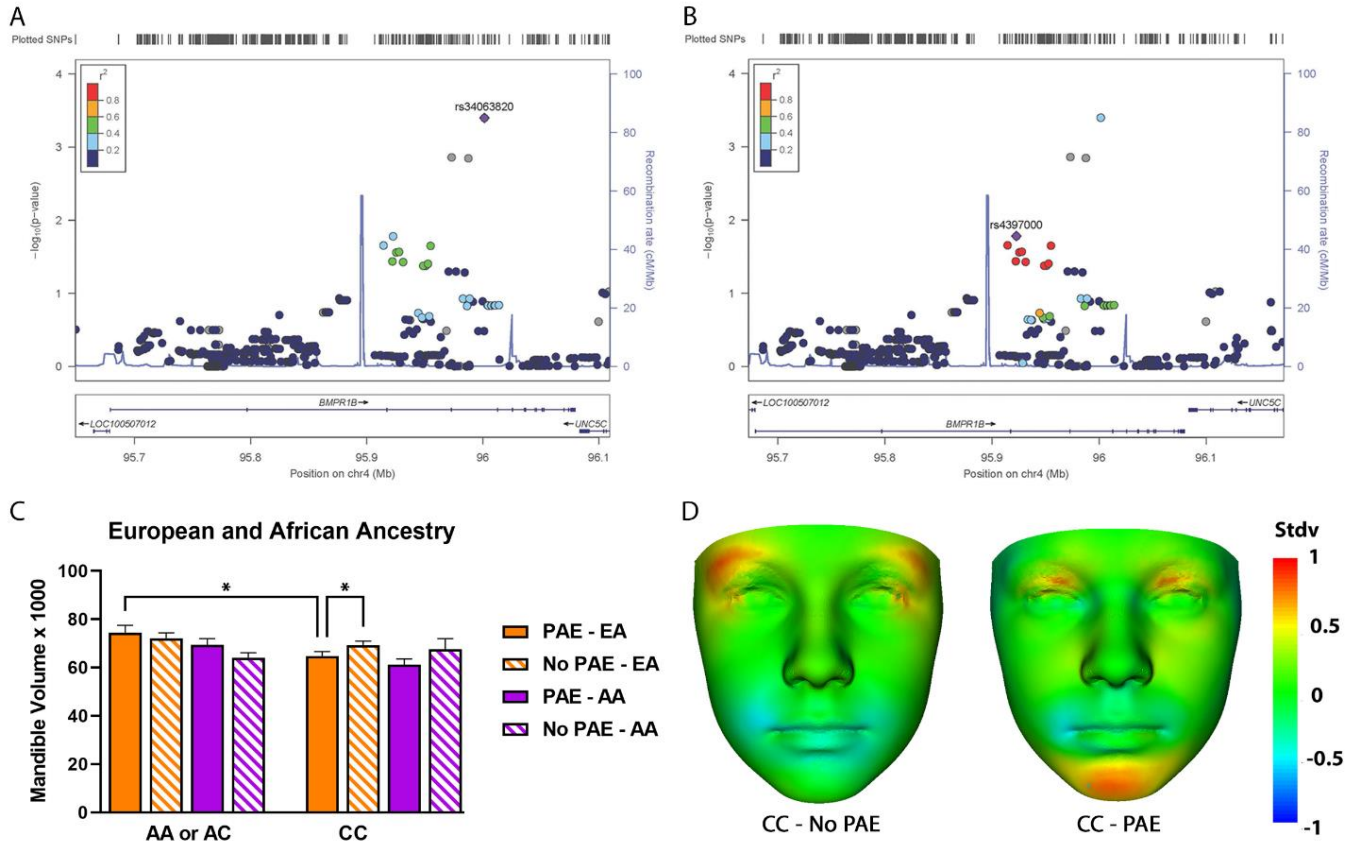


**Figure 6. Association of jaw deformations with SNPs located between BMPR1B in a combined European and African American discovery sample.** (**A-B**) Y-axis denotes the -log10 (p-value) for the genotype x PAE effect. X-axis is the physical position on the chromosome (Mb). The extent of linkage disequilibrium (as measured by r2) in the 1000 Genomes European reference panel between each SNP (circles) and the purple diamond SNP is indicated by the color scale at the top left. Larger values of r2 indicate greater linkage disequilibrium. (**A**) The SNP with the highest p-value in *BMPR1B*, *rs3406382*, is labeled with a purple diamond. (**B**) The cluster of nine SNPs in high LD with the purple diamond SNP *rs4397000*, and in lower LD with *rs3406382* (blue circle). SNP = single nucleotide polymorphism, PAE = prenatal alcohol exposure, LD = linkage disequilibrium. (**C**) Mandible volume in children of European and African ancestry (EA and AA, respectively) recruited with and without alcohol exposure according to genotype. In EA individuals with the *CC* genotype, mandible volume was significantly decreased in alcohol exposed vs unexposed individuals. In alcohol exposed EA individuals mandible volume was decreased in those with the *CC* genotype compared to those with the *AA+AC* genotypes. (**D**) DSM analysis facial signature heatmaps indicating surface to normal displacement at +/-1 s.d. for mean EA individuals. Where red-blue-green coloring indicates a reduction-expansion or agreement with the group being normalized against. (Left) *CC* genotype no PAE (n=52) normalized against *AA+AC* genotype no PAE (n=43). (Right) *CC* genotype with PAE (n=57), normalized against *AA+AC* genotype with PAE (n=28). Red coloring on the mandible's tip indicates a mandibular retraction or micrognathia. Mandible reduction is not observed without PAE. However, we do observe a red signal on the outer canthi, indicating a reduction in this region in the *CC* genotype group.

6C) had larger mandible volume on average than those with PAE (EA n=64, p=0.040; AA n=19, p=0.53). Furthermore, EA individuals with PAE with an *AA* or *AC* genotype had larger mandible volume than those who were *CC* (EA p=0.0058, AA p=0.108; Fig. 6C). A facial signature heatmap on the *CC* group normalized against the *AA* or *AC* group visualizes this volumetric reduction only when PAE is present, which is localized to the most anterior part of the mandible (Fig. 6D). Taken together, this genotype correlation with *BMPR1B* variants suggests that gene-ethanol interactions in the Bmp pathway potentially underlie abnormal jaw size in FASD, underlining the predictive value of our mechanistic studies underlying FASD etiology in zebrafish.

## Discussion

Formation of the facial skeleton is driven by a complex, highly coordinated, three-dimensional process involving multiple tissues in the developing head (16–18). Proper regulation of the cell movements and tissue dynamics within a single tissue and between different tissues are critical for these events (16–18). These cell behaviors are regulated by numerous signaling pathways, which can be attenuated either genetically and/or environmentally, leading to a cascading effect that disrupts craniofacial development (16–18). Prenatal ethanol exposure, defined as FASD, results in a highly variable set of phenotypes in the facial skeleton, including the jaw (6). Genetic risk factors are major drivers of FASD symptomology, providing insight into the cellular and molecular processes potentially disrupted in FASD (5).

### Bmp-ethanol interactions

Here, we show that mutation in several components of the Bmp pathway sensitize zebrafish embryos to ethanol induced malformations to the viscerocranium. We found that when exposed to ethanol from 10-18 hpf, mutations in *bmp2b*, *bmp4* and *bmpr1bb*, sensitize embryos to a range of ethanol-induced defects to Meckel's cartilages. These defects spanned outright loss of cartilage elements to reductions in cartilage size. Using a morphometric approach, we observed broad changes to facial shape in ethanol-treated Bmp mutants. Ethanol-treated larva displayed a shorter and wider face relative to untreated controls and a flattening of the angles of several cartilage elements. Much of this variation was not identified in our initial screens, supporting that this approach will identify subtle phenotypes impacting facial shape that would be missed if simply using linear measures of cartilage size (11,12,15). Importantly, these broad ethanol-induced facial

shape changes in zebrafish are consistent with analyses in human patients where alcohol exposed individuals showed broad and varied facial shaped changes compared to age-matched controls (7,45). Overall, our data documents that our morphometric analysis in zebrafish improve the rigor of identifying and quantifying ethanol-induced subtle facial shape changes, modeling the highly variable ethanol-induced facial shape changes in human studies.

Our results propose a synergistic interaction between Bmp and ethanol as neither condition alone generates the broad viscerocranial malformations observed in combination. Exacerbation of facial phenotypes in *bmp4*$^{-/-}$*;smad5*$^{-/-}$ larvae demonstrates that dose-dependent reduction in Bmp signaling drives ethanol-induced phenotypes, indicating that ethanol reduces signaling in the Bmp pathway. Work in mouse models of ethanol-induced iron deficiency found that ethanol decreases Bmp signaling (54,55). In these studies, ethanol exposure decreases phosphorylation levels of BmpR1 and Smad1,5 in the adult mouse liver. However, the gene expression levels of Bmp pathway components were contradictory with one study (Gerjevic et al., 2012) showed ethanol-induced increased gene expression of *Bmp2, Bmp4* and *Bmp6* (54), while the other study (Helfrich et al., 2023) showed ethanol-induced decreased gene expression of *Bmp2* and *Bmp6* (55). While our work and the mouse studies reveal that ethanol attenuates Bmp signaling, at what level and how ethanol disrupts Bmp signaling remains a major open question.

Work of multiple labs has shown that ethanol can disrupt cell signaling via direct molecular interactions (56). Ethanol interacts directly with several neurotransmitter receptors to alter their confirmation and subsequent function, resulting in altered receptor-ligand binding and/or downstream signaling responses (56). Multiple ethanol target sites have been identified in multiple domains in these large neurotransmitter receptors suggesting that ethanol could be interacting at one or multiple locations on Bmp signaling components. These ethanol-protein interactions would disrupt protein function of Bmp pathway components by interacting with and altering confirmation of these proteins disrupting pathway output. Through this mechanism, ethanol interaction could potentially disrupt ligand-receptor, receptor-receptor, receptor-Smad, Smad-Smad or Smad-DNA binding, attenuating downstream signaling.

Alternatively, ethanol may not interact with pathway components directly but could act either downstream of Bmp signaling impinging on target gene expression/function or on a parallel pathway, independent of, and concomitant with Bmp signaling. Ethanol can impact a number of epigenetic mechanisms, including chromatin modifications (57). Recent work has shown that the protein arginine methyltransferase PRMT1 can mediate Bmp-dependent Smad phosphorylation and DNA methylation regulating bone formation and suture closure in mice and ethanol has been shown to regulate both PRMT expression and function (58–60). This suggests that these epigenetic changes can disrupt the expression of Bmp target genes directly, modulating pathway function and target gene expression, or indirectly through methylation patterns that target expression of Bmp components and/or downstream targets. Additionally, these gene expression changes could extend beyond the Bmp pathway and its downstream targets, affecting parallel pathways necessary for craniofacial development. Ultimately, a holistic approach combining transcriptomic, proteomic and metabolomic methodologies investigating Bmp pathway components and downstream targets will be needed to further elucidate the interaction between ethanol and Bmp signaling during jaw formation.

**Impact of ethanol on pharyngeal endoderm morphogenesis**

Work in multiple model systems has shown that disruption to pharyngeal endoderm morphogenesis leads to jaw defects (19–23). This disruption alters the endodermal signaling centers that directly pattern the jaw leading to jaw hypoplasia (20,61,62). These signaling centers are critical for neural crest cell survival with disruptions to endoderm morphogenesis leading to neural crest cell death (63–65). We have previously shown that Bmp signaling is required for pharyngeal endoderm morphogenesis from 10-18 hpf, the same as our ethanol-sensitive time window, and blocking Bmp signaling with Dorsomorphin during this time window results in a wide range of defects to the viscerocranium (24). In addition, we observed an increase in cell death in tissues adjacent to the pharyngeal endoderm where neural crest populate suggesting that the Bmp-induced defects in endoderm morphogenesis are increasing cell death in the neural crest (24). Here, we show that our Bmp-ethanol interactions alter anterior pharyngeal endoderm shape, increasing the area of the anterior pharyngeal endoderm relative to head size. Strikingly, this increase in anterior pharyngeal endoderm size stands at odds with the decreases we observed in jaw shape and size. This has been previously observed in morpholino knockdown of *vgll2a*, which results in shorter and wider endodermal pouches but viscerocranial hypoplasia as a result of increased neural crest cell death (64). It is possible that ethanol-

induced increases in anterior endoderm size disrupt endodermal signaling centers leading to neural crest cell death. This results in decreased neural crest cell contribution to the forming jaw decreasing its size. However, future work examining endoderm-induced neural crest cell death will need to be properly controlled as ethanol exposure is known to induce neural crest cell death directly (11,66).

While the anterior pharyngeal endoderm signals directly to the cranial neural crest for cell survival, the signaling can also be indirect, by inducing oral ectoderm signaling factor expression which is critical for jaw formation (19,22,23). These tripartite tissue interactions can be highly variable with endoderm mutants showing both reductions and expansion in oral ectoderm signaling centers and resultant hyper- and hypoplasia of the viscerocranium (19). Here, we show that, in addition to endodermal defects, blocking Bmp signaling with Dorsomorphin leads to variable disruption of *fgf8a* expression in the oral ectoderm. Strikingly, expression of *fgf8a* in the oral ectoderm was expanded in ethanol-treated *bmp4*$^{-/-}$*;smad5*$^{-/-}$ embryos. Though consistent with the increase in anterior pharyngeal endoderm size, this stands at odds with disruption of Bmp signaling. This suggests that the Bmp-ethanol interaction disrupts jaw formation through an endoderm-oral ectoderm-neural crest signaling axis. However, how this increase in size in both anterior pharyngeal endoderm and oral ectoderm signaling centers differs from Dorsomorphin blockade of Bmp signaling and still results in a smaller jaw in ethanol-treated Bmp mutants remains unclear. Both, the oral ectoderm and surrounding neural crest express a number of signaling factors that drive jaw and palate formation (50). Changes in the expression domain of any number of these could disrupt local interaction points between the neural crest and oral ectoderm resulting in jaw malformations (19). While our data supports the hypothesis that Bmp-ethanol interactions disrupt an endoderm-oral ectoderm-neural crest-signaling axis, more work needs to be done to analyze the impact of ethanol on these tripartite interactions driving jaw formation and the cell behaviors that establish these interactions.

**Zebrafish model gene-ethanol interactions in human FASD**

We have previously shown that our zebrafish screens can predict gene-ethanol interactions in humans suggesting that our Bmp-ethanol interactions impacting facial shape may also be predictive of gene-ethanol associations in humans (11). Consistent with this, disruption of *Bmp2* (*BMP2*) in both mice and humans, *in the absence of ethanol*, result in a hypoplastic jaw (67,68). From a study of children recruited with and

without PAE, we show here that several SNPs in *BMPR1B* are significantly associated with ethanol-associated jaw malformations. Jaw hypoplasia is commonly observed in FASD (6,7,69) but studying FASD in humans is incredibly challenging due to the complex interplay between genetic background and ethanol timing and dosage. Our results show that zebrafish analyses can model gene-ethanol associations in humans, strongly phenocopying both the malformation and the variation inherent in human data (7,11,70). However, due to the paucity of human genetic studies of FASD, sample sizes with sufficient power to detect association due to the effect of multiple genes in one epistatic model is currently not possible. Thus, the zebrafish model remains a powerful, efficient method to simultaneously examine the effect of multiple genes on facial measures and to generate a deeper mechanistic understanding of these gene-ethanol interactions on craniofacial development. While future functional human and zebrafish analyses will need to test for the causal relationship and mechanistic underpinnings of ethanol-induced jaw deformations, this work strongly suggests that jaw malformations in FASD may in part be due to disruptions to epithelial dynamics and signaling events.

Combined, our results show that zebrafish can predict Bmp-ethanol associations in human and provide a valuable model system for determining the ethanol-sensitive tissue events that contribute to facial defects in FASD. However, despite our increased understanding of the clinical impact of prenatal ethanol exposure, much remains to be learned of the cellular mechanisms underlying FASD (5). Our work here provides some of the first evidence of gene-ethanol interactions altering epithelial dynamics in the complex, endoderm-oral ectoderm-neural crest-signaling axis leading to facial malformations. This expands our current understanding of ethanol-sensitive tissue dynamics in FASD and provides a conceptual framework for future FASD studies. Ultimately, this work generates a mechanistic paradigm of ethanol-induced structural birth defects and connects ethanol exposure with concrete cellular events that could be sensitive beyond the jaw.

## Materials and Methods

### Zebrafish (*Danio rerio*) care and use

All zebrafish were raised and cared for using established IACUC protocols approved by the University of Louisville (71). Adult fish were maintained at 28.5°C with a 14 / 10-hour light / dark cycle. The *bmp2b*$^{tc300a}$

(72), *bmp4*$^{st72}$ (73), *bmpr1bb*$^{sw40}$ (32) and *smad5*$^{b1100}$ (50) and *sox17:EGFP*$^{s870}$ (74) zebrafish lines were previously described.

**Zebrafish staging and ethanol treatment**

Eggs were collected and embryos were morphologically staged (71), sorted into sample groups of 100 and reared at 28.5°C to desired developmental time points. All groups were incubated in embryo media (EM). At 10 hpf, EM was changed to either fresh EM or EM containing 1% ethanol (v/v). At 18 hpf, EM containing ethanol was washed out with 3 fresh changes of EM.

**Hybridization chain reaction (HCR), immunofluorescence and in situ hybridization**

Embryos were collected at 36 hpf, dechorionated and fixed in 4% paraformaldehyde/PBS at 4°C. HCR protocol was previously described (75). HCR amplifiers and buffers were acquired from Molecular Instruments (Molecular Instruments). HCR probes against *fgf8a* were designed as previously described (76). Immunofluorescence was performed as previously described (24). Primary antibody was anti-GFP (sc-9996, Santa Cruz), secondary antibody was Alexa Fluor 488 (A10042, Invitrogen). RNA in situ hybridization was performed as previously described (77) and mRNA probes against *fgf8a* (78), *pdgfaa* and *pdgfab* (79) were described previously.

**Imaging & analysis of anterior pharyngeal endoderm shape**

Confocal images were taken using an Olympus FV1000 microscope and measured in FIJI (80). The anterior pharyngeal endoderm was defined as the medial endoderm anterior to the first pouch. General head area was defined as the product of the width and length of the embryo anterior to the first pouch.

**Cartilage and Bone staining**

Zebrafish larva fixed at 5 dpf were stained with alcian blue for cartilage and alizarin red for bone (81). Whole mount, ventral view, brightfield images of the viscerocranium were taken on an Olympus BX53 compound microscope.

**Morphometric analyses**

Morphometric analysis of alcian/alizarin-stained larva was performed in TpsDig2 (https://sbmorphomectrics.org) and MorphoJ (82). Landmarks were placed on the following joints, Meckel's cartilage midline joint, the joints between Meckels' and the palatoquadrate, the palatoquadrate and ceratohyal and at the end of the hyomandibular cartilages. Linear measures were analyzed using TpsDig2. Principle component analysis (PCA), Procrustes ANOVA and wireframe graphs of facial variation were generated using MorphoJ.

**Statistical analyses**

Meckel's cartilage area was analyzed with a one-way ANOVA with a Tukey's Multiple Comparisons Test. Area measures of the anterior endoderm/head and linear measures/angles of both the anterior endoderm and Alcian/alizarin-stained viscerocranium were analyzed with a two-way ANOVA (type III) with a Tukey's Multiple Comparisons Test in Graphpad Prism 9.5.1 (Graphpad Software Inc., La Jolla, CA).

**Human Studies**

Human participants were recruited as part of the Collaborative Initiative on FASD (CIFASD) from (2007-2017) from sites in Atlanta, GA, Los Angeles, CA, Minneapolis, MN, and San Diego, CA (83,84). Institutional Review Board approval was obtained at each site. All participants and/or their parents/legal guardians provided written informed consent and Institutional Review Board approval was obtained at each recruiting site. Children (aged 5-18 years) who experienced heavy (>4 drinks/occasion at least weekly or >13 drinks/week) prenatal alcohol exposure (PAE) with or without a diagnosis of FAS were classified as PAE, and those who were exposed to minimal (<1 drink/week or <2 drinks/occasion) or no PAE were classified as no PAE (83,84). 3D images were obtained on most participants at the time of the dysmorphology exam using static stereophotogrammetric camera systems capable of capturing a 180-degree image of facial surface geometry. Images were annotated with a sparse set of 20 reliable anthropometric landmarks (Supplement Fig. 1A). We performed a Procrustes alignment on the landmarks of each face, aligning them to a template face using a similarity transform, which was applied to each 3D surface to normalize size to a uniform scale. Dense surface models (DSMs) have been used for the assessment of subtle facial dysmorphia across the FASD spectrum (7,70), and provide a method to assess surface-based differences of 3D structures, and compare groups of individuals to assess mean differences. A DSM

containing 303 individuals was constructed from the uniformly scaled images to produce shape only morphometric models. DSMs allow us to compute facial signatures, which represent normalized differences between groups, and visualize using a heatmap representation group or individual differences (85). To evaluate micrognathia, we computed mandible volume, which was outlined and validated against CT images in (69). This technique estimated the volume of a trapezoid formed by four specific points on the size-normalized face: the left and right lower otobasion inferius (lowest points of the ears), gnathion (tip of the mandible), and lower lip vermillion center (Supplement Fig. 1B).

Genome-wide association study (GWAS) data were genotyped on the OmniExpress genome array (Illumina, San Diego CA) and on the Multi-Ethnic Genotyping Array at the Johns Hopkins Genetic Resources Core Facility (Baltimore, MD; Dou et al., 2018). Following a previously published GWAS cleaning pipeline (87), the two datasets were cleaned for sample and variant call rates, Hardy-Weinberg Equilibrium (HWE), sample identity using genetic (calculated from single nucleotide polymorphisms [SNPs] on X and Y chromosomes) and self-reported sex, sample relatedness, and genetic ancestry. The two cleaned datasets were imputed separately using Michigan Imputation Server (88) to 1000-Genomes Phase 3, b37 reference panel (89) then combined. The final dataset consisted of 4,000,362 genotyped and imputed SNPs with minor allele frequency (MAF) $\geq 0.01$, genotype rate $\geq 0.99$, and Hardy-Weinberg equilibrium $p \geq 0.000001$. Principal components analysis (PCA) was performed using SNPRelate (90) with genotype data from autosomes. Individuals in the 1000-Genomes database (89) were included as reference samples for clustering individuals based on genetic ancestry similarities. Individuals were grouped with European Ancestry (EA, n=222), African Ancestry (AA, n=103) or other (n=44) ancestry samples from 1000 Genomes Project using the first three principal components. Only EA and AA individuals were included in our analyses.

Analyses were performed separately in the EA and AA groups using R (version 4.2.0; R Foundation for Statistical Computing; http://cran.r-project.org/) and PLINK v2.00a3 64-bit (8 Jun 2021). Association of SNP genotype with mandible volume was assessed using an additive generalized linear model with sex, age at time of 3D image, the first 10 genetic principal components, genotype, PAE and genotype by PAE interaction. As the effect of interest was the association of genotype with mandible volume with and without

the presence of PAE, the p-value for the genotype by PAE interaction is reported. Variants within 25 kilobase pairs of the three genes of interest (*BMP2, BMP4, BMPR1B*) were evaluated in the EA group to identify significant SNPs ($p<0.05$). To further explore the genotype by PAE interaction, we employed a non-parametric Wilcoxon test (SAS v 9.4) to compare mandible volume in individuals with PAE to those without PAE stratified by genotype, and to compare mandible volume by genotype groups stratified by PAE. All analyses were performed in the EA and AA samples separately.

**Acknowledgements**

The authors like to thank Kevin Kump for animal care and husbandry. We thank Dr. Jim Amatruda for the providing the *bmpr1bb* zebrafish line. We also thank Dr. Duygu Özpolat and Dr. Ryan Hull for providing script for HCR probe design. We thank Dr. Christian Mosimann for external manuscript editing. Data used in preparation of this article were obtained in conjunction with the Collaborative Initiative on Fetal Alcohol Spectrum Disorders (CIFASD; https://cifasd.org/data-sharing/) supported by the National Institute of Alcohol Abuse and Alcoholism.

**Funding**

National Institutes of Health/National Institute on Alcohol Abuse (NIH/NIAAA) R00AA023560 (CBL).

National Institutes of Health/National Institute on Alcohol Abuse (NIH/NIAAA) U01AA014809 and U01AA025103 (TF).

National Institutes of Health/National Institute on Alcohol Abuse (NIH/NIAAA) U24AA030169 (LW).

National Institutes of Health/National Institute on Alcohol Abuse (NIH/NIAAA) U01AA014809 (MS).

**Author Contributions**

CBL conceived the project. JRK and CBL designed all zebrafish studies. JRK, RG, HV, GC and CBL conducted all zebrafish experiments. JRK and CBL analyzed zebrafish data and generated all zebrafish figures. LW, TS, MA and MS designed all human studies and analyzed human data. LW and MS generated human figures. JLK and CBL wrote the manuscript. LW, MS, JLK and CBL reviewed and edited the manuscript. All authors have read and approved the final manuscript.

**Conflicts of Interest**

The authors declare that they have no competing interests.

**Data and materials availability**

All data needed to evaluate the conclusions in the paper are present in the paper and/or the Supplementary Materials. The human genetic data utilized in the CIFASD cohort are available at https://cifasd.org/data-sharing/.

## References


1. May PA, Chambers CD, Kalberg WO, Zellner J, Feldman H, Buckley D, et al. Prevalence of Fetal Alcohol Spectrum Disorders in 4 US Communities. JAMA. 2018 Feb 6;319(5):474.

2. Popova S, Lange S, Shield K, Burd L, Rehm J. Prevalence of fetal alcohol spectrum disorder among special subpopulations: a systematic review and meta-analysis. Addiction. 2019 Jul;114(7):1150–72.

3. Finer LB, Zolna MR. Declines in Unintended Pregnancy in the United States, 2008–2011. N Engl J Med. 2016 Mar 3;374(9):843–52.

4. Rojmahamongkol P, Cheema-Hasan A, Weitzman C. Do Pediatricians Recognize Fetal Alcohol Spectrum Disorders in Children With Developmental and Behavioral Problems? Journal of Developmental & Behavioral Pediatrics. 2015 Apr;36(3):197–202.

5. Lovely CB. Animal models of gene–alcohol interactions. Birth Defects Research. 2020 Mar;112(4):367–79.

6. Blanck-Lubarsch M, Dirksen D, Feldmann R, Sauerland C, Kirschneck C, Hohoff A. Asymmetry-index and orthodontic facial analysis of children with foetal alcohol syndrome using 3D-facial scans. Pediatr Res. 2020 Aug;88(2):243–9.

7. Suttie M, Foroud T, Wetherill L, Jacobson JL, Molteno CD, Meintjes EM, et al. Facial Dysmorphism Across the Fetal Alcohol Spectrum. 2013;131(3):12.

8. Muggli E, Matthews H, Penington A, Claes P, O'Leary C, Forster D, et al. Association Between Prenatal Alcohol Exposure and Craniofacial Shape of Children at 12 Months of Age. JAMA Pediatr. 2017 Aug 1;171(8):771.

9. Boyles AL, DeRoo LA, Lie RT, Taylor JA, Jugessur A, Murray JC, et al. Maternal Alcohol Consumption, Alcohol Metabolism Genes, and the Risk of Oral Clefts: A Population-based Case-Control Study in Norway, 1996-2001. American Journal of Epidemiology. 2010 Oct 15;172(8):924–31.

10. Hong M, Krauss RS. Cdon Mutation and Fetal Ethanol Exposure Synergize to Produce Midline Signaling Defects and Holoprosencephaly Spectrum Disorders in Mice. Hébert JM, editor. PLoS Genet. 2012 Oct 11;8(10):e1002999.

11. McCarthy N, Wetherill L, Lovely CB, Swartz ME, Foroud TM, Eberhart JK. Pdgfra protects against ethanol-induced craniofacial defects in a zebrafish model of FASD. Development. 2013 Aug 1;140(15):3254–65.

12. Swartz ME, Wells MB, Griffin M, McCarthy N, Lovely CB, McGurk P, et al. A Screen of Zebrafish Mutants Identifies Ethanol-Sensitive Genetic Loci. Alcohol Clin Exp Res. 2014 Mar;38(3):694–703.

13. Zhang C, Ojiaku P, Cole GJ. Forebrain and hindbrain development in zebrafish is sensitive to ethanol exposure involving agrin, Fgf, and sonic hedgehog function. Birth Defects Research Part A: Clinical and Molecular Teratology. 2013 Jan;97(1):8–27.

14. Fernandes Y, Lovely CB. Zebrafish models of fetal alcohol spectrum disorders. genesis [Internet]. 2021 Nov [cited 2022 Jan 19];59(11). Available from: https://onlinelibrary.wiley.com/doi/10.1002/dvg.23460

15. Swartz ME, Lovely CB, McCarthy N, Kuka T, Eberhart JK. Novel Ethanol-Sensitive Mutants Identified in an F3 Forward Genetic Screen. Alcohol Clin Exp Res. 2020 Jan;44(1):56–65.

16. Knight RD, Schilling TF. Cranial Neural Crest and Development of the Head Skeleton. In: Saint-Jeannet JP, editor. Neural Crest Induction and Differentiation [Internet]. Boston, MA: Springer US; 2006 [cited 2021 Feb 23]. p. 120–33. (Advances in Experimental Medicine and Biology; vol. 589). Available from: http://link.springer.com/10.1007/978-0-387-46954-6_7

17. Medeiros DM, Crump JG. New perspectives on pharyngeal dorsoventral patterning in development and evolution of the vertebrate jaw. Developmental Biology. 2012 Nov;371(2):121–35.

18. Murillo-Rincón AP, Kaucka M. Insights Into the Complexity of Craniofacial Development From a Cellular Perspective. Front Cell Dev Biol. 2020 Dec 18;8:620735.

19. Balczerski B, Matsutani M, Castillo P, Osborne N, Stainier DYR, Crump JG. Analysis of Sphingosine-1-phosphate signaling mutants reveals endodermal requirements for the growth but not dorsoventral patterning of jaw skeletal precursors. Developmental Biology. 2012 Feb;362(2):230–41.

20. Couly G, Creuzet S, Bennaceur S, Vincent C, Le Douarin NM. Interactions between Hox-negative cephalic neural crest cells and the foregut endoderm in patterning the facial skeleton in the vertebrate head. Development. 2002 Feb;129(4):1061–73.

21. Crump JG. An essential role for Fgfs in endodermal pouch formation influences later craniofacial skeletal patterning. Development. 2004 Nov 15;131(22):5703–16.

22. Haworth KE, Wilson JM, Grevellec A, Cobourne MT, Healy C, Helms JA, et al. Sonic hedgehog in the pharyngeal endoderm controls arch pattern via regulation of Fgf8 in head ectoderm. Developmental Biology. 2007 Mar;303(1):244–58.

23. Haworth KE, Healy C, Morgan P, Sharpe PT. Regionalisation of early head ectoderm is regulated by endoderm and prepatterns the orofacial epithelium. Development. 2004 Oct 1;131(19):4797–806.

24. Lovely CB, Swartz ME, McCarthy N, Norrie JL, Eberhart JK. Bmp signaling mediates endoderm pouch morphogenesis by regulating Fgf signaling in zebrafish. Development. 2016 Jun 1;143(11):2000–11.

25. Choe CP, Collazo A, Trinh LA, Pan L, Moens CB, Crump JG. Wnt-Dependent Epithelial Transitions Drive Pharyngeal Pouch Formation. Developmental Cell. 2013 Feb;24(3):296–309.

26. Choe CP, Crump JG. Tbx1 controls the morphogenesis of pharyngeal pouch epithelia through mesodermal Wnt11r and Fgf8a. Development. 2014 Sep 15;141(18):3583–93.

27. Hu B, Gao Y, Davies L, Woo S, Topczewski J, Jessen JR, et al. Glypican 4 and Mmp14 interact in regulating the migration of anterior endodermal cells by limiting extracellular matrix deposition. Development. 2018 Sep 1;145(17):dev163303.

28. Li L, Ning G, Yang S, Yan Y, Cao Y, Wang Q. BMP signaling is required for nkx2.3-positive pharyngeal pouch progenitor specification in zebrafish. Moens C, editor. PLoS Genet. 2019 Feb 14;15(2):e1007996.

29. Kondo M. Bone morphogenetic proteins in the early development of zebrafish: BMPs in the early development of zebrafish. FEBS Journal. 2007 Jun;274(12):2960–7.

30. Little SC, Mullins MC. Bone morphogenetic protein heterodimers assemble heteromeric type I receptor complexes to pattern the dorsoventral axis. Nat Cell Biol. 2009 May;11(5):637–43.

31. Tajer B, Dutko JA, Little SC, Mullins MC. BMP heterodimers signal via distinct type I receptor class functions. Proc Natl Acad Sci USA. 2021 Apr 13;118(15):e2017952118.

32. Neumann JC, Chandler GL, Damoulis VA, Fustino NJ, Lillard K, Looijenga L, et al. Mutation in the type IB bone morphogenetic protein receptor *alk6b* impairs germ-cell differentiation and causes germ-cell tumors in zebrafish. Proc Natl Acad Sci USA. 2011 Aug 9;108(32):13153–8.

33. Bilotta J, Barnett JA, Hancock L, Saszik S. Ethanol exposure alters zebrafish development: A novel model of fetal alcohol syndrome. Neurotoxicology and Teratology. 2004 Nov;26(6):737–43.

34. Everson JL, Tseng Y, Eberhart JK. High-throughput detection of craniofacial defects in fluorescent zebrafish. Birth Defects Research. 2022 Nov 11;bdr2.2127.

35. Zhang C, Frazier JM, Chen H, Liu Y, Lee JA, Cole GJ. Molecular and morphological changes in zebrafish following transient ethanol exposure during defined developmental stages. Neurotoxicology and Teratology. 2014 Jul;44:70–80.

36. Flentke GR, Klingler RH, Tanguay RL, Carvan MJ, Smith SM. An Evolutionarily Conserved Mechanism of Calcium-Dependent Neurotoxicity in a Zebrafish Model of Fetal Alcohol Spectrum Disorders. Alcohol Clin Exp Res. 2014 May;38(5):1255–65.

37. Lovely CB, Nobles RD, Eberhart JK. Developmental age strengthens barriers to ethanol accumulation in zebrafish. Alcohol. 2014 Sep;48(6):595–602.

38. Reimers MJ, Flockton AR, Tanguay RL. Ethanol- and acetaldehyde-mediated developmental toxicity in zebrafish. Neurotoxicology and Teratology. 2004 Nov;26(6):769–81.

39. Maier SE. Drinking Patterns and Alcohol-Related Birth Defects. 2001;25(3):7.

40. Ethen MK, Ramadhani TA, Scheuerle AE, Canfield MA, Wyszynski DF, Druschel CM, et al. Alcohol Consumption by Women Before and During Pregnancy. Matern Child Health J. 2009 Mar;13(2):274–85.

41. Canfield DV, Forster EM, Cheong ZI, Cowan JM. Breath/Blood Alcohol Concentration as an Indicator of Alcohol Use Problems. Aerospace Medicine and Human Performance. 2019 May 1;90(5):488–91.

42. Jones AW. Ultra-rapid rate of ethanol elimination from blood in drunken drivers with extremely high blood-alcohol concentrations. Int J Legal Med. 2008 Mar;122(2):129–34.

43. Whaley CC, Young MM, Gaynor BG. Very High Blood Alcohol Concentration and Fatal Hemorrhage in Acute Subdural Hematoma. World Neurosurgery. 2019 Oct;130:454–8.

44. Nguyen VH, Schmid B, Trout J, Connors SA, Ekker M, Mullins MC. Ventral and Lateral Regions of the Zebrafish Gastrula, Including the Neural Crest Progenitors, Are Established by abmp2b/swirlPathway of Genes. Developmental Biology. 1998 Jul;199(1):93–110.

45. Bemquerer LM, Gomes IA, Sodr F. Orofacial Manifestations of Fetal Alcohol Syndrome: Two Case Reports and a Scoping Review. Journal of Dentistry for Children. 2022;

46. Li L, Lin M, Wang Y, Cserjesi P, Chen Z, Chen Y. BmprIa is required in mesenchymal tissue and has limited redundant function with BmprIb in tooth and palate development. Developmental Biology. 2011 Jan;349(2):451–61.

47. Mu H, Liu X, Geng S, Su D, Chang H, Li L, et al. Epithelial Bone Morphogenic Protein 2 and 4 Are Indispensable for Tooth Development. Front Physiol. 2021 Aug 16;12:660644.

48. Schille C, Heller J, Schambony A. Differential requirement of bone morphogenetic protein receptors Ia (ALK3) and Ib (ALK6) in early embryonic patterning and neural crest development. BMC Dev Biol. 2016 Jan 19;16(1):1.

49. Wise SB, Stock DW. bmp2b and bmp4 are dispensable for zebrafish tooth development. Dev Dyn. 2010 Sep 20;239(10):2534–46.

50. Swartz ME, Sheehan-Rooney K, Dixon MJ, Eberhart JK. Examination of a palatogenic gene program in zebrafish. Dev Dyn. 2011 Sep;240(9):2204–20.

51. Chung WS, Stainier DYR. Intra-Endodermal Interactions Are Required for Pancreatic β Cell Induction. Developmental Cell. 2008 Apr;14(4):582–93.

52. Lieschke GJ, Currie PD. Animal models of human disease: zebrafish swim into view. Nat Rev Genet. 2007 May;8(5):353–67.

53. Santoriello C, Zon LI. Hooked! Modeling human disease in zebrafish. J Clin Invest. 2012 Jul 2;122(7):2337–43.

54. Gerjevic LN, Liu N, Lu S, Harrison-Findik DD. Alcohol Activates TGF-Beta but Inhibits BMP Receptor-Mediated Smad Signaling and Smad4 Binding to Hepcidin Promoter in the Liver. International Journal of Hepatology. 2012;2012:1–11.

55. Helfrich KK, Saini N, Kwan ST, Rivera OC, Mooney SM, Smith SM. Fetal anemia and elevated hepcidin in a mouse model of fetal alcohol spectrum disorder. Pediatr Res. 2023 Aug;94(2):503–11.

56. Abrahao KP, Salinas AG, Lovinger DM. Alcohol and the Brain: Neuronal Molecular Targets, Synapses, and Circuits. Neuron. 2017 Dec;96(6):1223–38.

57. Zakhari S. Alcohol Metabolism and Epigenetics Changes. 2013;

58. Hashimoto JG, Gavin DP, Wiren KM, Crabbe JC, Guizzetti M. Prefrontal cortex expression of chromatin modifier genes in male WSP and WSR mice changes across ethanol dependence, withdrawal, and abstinence. Alcohol. 2017 May;60:83–94.

59. Ye H, Cao L, Jackson-Weaver O, Zheng L, Gou Y. PRMT1-mediated arginine methylation promotes postnatal calvaria bone formation through BMP-Smad signaling. Bone. 2023 Aug;116887.

60. Zhao J, Adams A, Weinman SA, Tikhanovich I. Hepatocyte PRMT1 protects from alcohol induced liver injury by modulating oxidative stress responses. Sci Rep. 2019 Jun 24;9(1):9111.

61. Suzuki T, Oohara I, Kurokawa T. Retinoic acid given at late embryonic stage depresses sonic hedgehog and Hoxd-4 expression in the pharyngeal area and induces skeletal malformation in flounder (Paralichthys olivaceus) embryos. Dev Growth Differ. 1999 Apr;41(2):143–52.

62. Vieux-Rochas M, Mantero S, Heude E, Barbieri O, Astigiano S, Couly G, et al. Spatio-temporal dynamics of gene expression of the Edn1-Dlx5/6 pathway during development of the lower jaw. Genesis. 2010 Mar 23;48(6):262–373.

63. Edlund RK, Ohyama T, Kantarci H, Riley BB, Groves AK. Foxi transcription factors promote pharyngeal arch development by regulating formation of FGF signaling centers. Developmental Biology. 2014 Jun;390(1):1–13.

64. Johnson CW, Hernandez-Lagunas L, Feng W, Melvin VS, Williams T, Artinger KB. Vgll2a is required for neural crest cell survival during zebrafish craniofacial development. Developmental Biology. 2011 Sep;357(1):269–81.

65. Kopinke D, Sasine J, Swift J, Stephens WZ, Piotrowski T. Retinoic acid is required for endodermal pouch morphogenesis and not for pharyngeal endoderm specification. Dev Dyn. 2006 Oct;235(10):2695–709.

66. Dunty WC, Chen S yu, Zucker RM, Dehart DB, Sulik KK. Selective Vulnerability of Embryonic Cell Populations to Ethanol-Induced Apoptosis: Implications for Alcohol-Related Birth Defects and Neurodevelopmental Disorder. Alcoholism Clin Exp Res. 2001 Oct;25(10):1523–35.

67. Sahoo T, Theisen A, Sanchez-Lara PA, Marble M, Schweitzer DN, Torchia BS, et al. Microdeletion 20p12.3 involving BMP2 contributes to syndromic forms of cleft palate. Am J Med Genet. 2011 Jul;155(7):1646–53.

68. Chen Y, Wang Z, Chen Y, Zhang Y. Conditional deletion of Bmp2 in cranial neural crest cells recapitulates Pierre Robin sequence in mice. Cell Tissue Res. 2019 May;376(2):199–210.

69. Basart H, Suttie M, Ibrahim A, Ferretti P, Van Der Horst CMAM, Hennekam RC, et al. Objectifying Micrognathia Using Three-Dimensional Photogrammetric Analysis: Journal of Craniofacial Surgery. 2018 Nov;29(8):2106–9.

70. Suttie M, Wetherill L, Jacobson SW, Jacobson JL, Hoyme HE, Sowell ER, et al. Facial Curvature Detects and Explicates Ethnic Differences in Effects of Prenatal Alcohol Exposure. Alcohol Clin Exp Res. 2017 Aug;41(8):1471–83.

71. Westerfield M. The zebrafish book. A guide for the laboratory use of zebrafish (Danio rerio). 5th ed. 2007.

72. Mullins MC, Hammerschmidt M, Kane DA, Odenthal J, Brand M. Genes establishing dorsoventral pattern formation in the zebrafish embryo: the ventral specifying genes. Development. 1996;123:13.

73. Stickney HL, Imai Y, Draper B, Moens C, Talbot WS. Zebrafish bmp4 functions during late gastrulation to specify ventroposterior cell fates. Developmental Biology. 2007;14.

74. Chung WS, Stainier DYR. Intra-Endodermal Interactions Are Required for Pancreatic β Cell Induction. Developmental Cell. 2008 Apr;14(4):582–93.

75. Ibarra-García-Padilla R, Howard AGA, Singleton EW, Uribe RA. A protocol for whole-mount immuno-coupled hybridization chain reaction (WICHCR) in zebrafish embryos and larvae. STAR Protocols. 2021;2(3):100709.

76. Kuehn E, Clausen DS, Null RW, Metzger BM, Willis AD, Özpolat BD. Segment number threshold determines juvenile onset of germline cluster expansion in *Platynereis dumerilii*. J Exp Zool Pt B. 2022 Jun;338(4):225–40.

77. Miller CT, Schilling, TF, Lee, KH, Parker J, Kimmel CB. *sucker* encodes a zebrafish Endothelin-1 required for ventral pharyngeal arch development. Development. 2000 Sep 1;127(17):3815–28.

78. Reifers F, Walsh EC, Léger S, Stainier DYR, Brand M. Induction and differentiation of the zebrafish heart requires fibroblast growth factor 8 ( *fgf8/acerebellar* ). Development. 2000 Jan 15;127(2):225–35.

79. Eberhart JK, He X, Swartz ME, Yan YL, Song H, Boling TC, et al. MicroRNA Mirn140 modulates Pdgf signaling during palatogenesis. Nat Genet. 2008 Mar;40(3):290–8.

80. Schindelin J, Arganda-Carreras I, Frise E, Kaynig V, Longair M, Pietzsch T, et al. Fiji: an open-source platform for biological-image analysis. Nat Methods. 2012 Jul;9(7):676–82.

81. Walker M, Kimmel C. A two-color acid-free cartilage and bone stain for zebrafish larvae. Biotechnic & Histochemistry. 2007 Jan;82(1):23–8.

82. Klingenberg CP. MorphoJ: an integrated software package for geometric morphometrics: COMPUTER PROGRAM NOTE. Molecular Ecology Resources. 2011 Mar;11(2):353–7.

83. Mattson SN, Foroud T, Sowell ER, Jones KL, Coles CD, Fagerlund Å, et al. Collaborative initiative on fetal alcohol spectrum disorders: methodology of clinical projects. Alcohol. 2010 Nov;44(7–8):635–41.

84. Mattson SN, Roesch SC, Fagerlund Å, Autti-Rämö I, Jones KL, May PA, et al. Toward a Neurobehavioral Profile of Fetal Alcohol Spectrum Disorders: NEUROBEHAVIORAL PROFILE OF

FETAL ALCOHOL SPECTRUM DISORDERS. Alcoholism: Clinical and Experimental Research. 2010 Sep;34(9):1640–50.

85. Hammond P, Suttie M, Hennekam RC, Allanson J, Shore EM, Kaplan FS. The face signature of fibrodysplasia ossificans progressiva. Am J Med Genet. 2012 Jun;158A(6):1368–80.

86. Dou X, Menkari C, Mitsuyama R, Foroud T, Wetherill L, Hammond P, et al. L1 coupling to ankyrin and the spectrin-actin cytoskeleton modulates ethanol inhibition of L1 adhesion and ethanol teratogenesis. FASEB j. 2018 Mar;32(3):1364–74.

87. Schwantes-An T, Darlay R, Mathurin P, Masson S, Liangpunsakul S, Mueller S, et al. Genome-wide Association Study and Meta-analysis on Alcohol-Associated Liver Cirrhosis Identifies Genetic Risk Factors. Hepatology. 2021 May;73(5):1920–31.

88. Das S, Forer L, Schönherr S, Sidore C, Locke AE, Kwong A, et al. Next-generation genotype imputation service and methods. Nat Genet. 2016 Oct;48(10):1284–7.

89. Fairley S, Lowy-Gallego E, Perry E, Flicek P. The International Genome Sample Resource (IGSR) collection of open human genomic variation resources. Nucleic Acids Research. 2020 Jan 8;48(D1):D941–7.

90. Zheng X, Levine D, Shen J, Gogarten SM, Laurie C, Weir BS. A high-performance computing toolset for relatedness and principal component analysis of SNP data. Bioinformatics. 2012 Dec 1;28(24):3326–8.

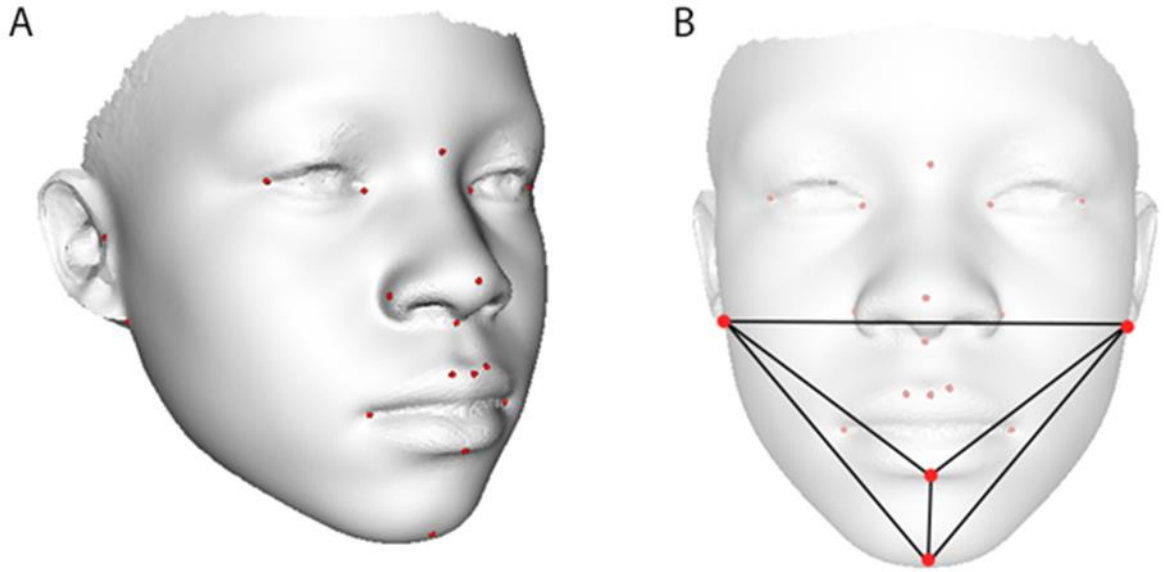


**Supplemental Figure 1. Visual representation of the 20 landmark locations used to induce the dense surface correspondence.** (**A-B**) left and right endocanthion, exocanthion, tragion, otobasion inferius, crista philtrum, cheilion, and alare; nasion, pronasale, subnasale, labiale superius, labiale inferius, and gnathion. (**B**) The landmarks labiuminferius, gnathion, and otobasion inferior define the tetrahedron (1,2,3,4). The volume of the tetrahedron is calculated as (1/6)det (axayaz1; bxbybz1; cxcycz1; dxdydz1).

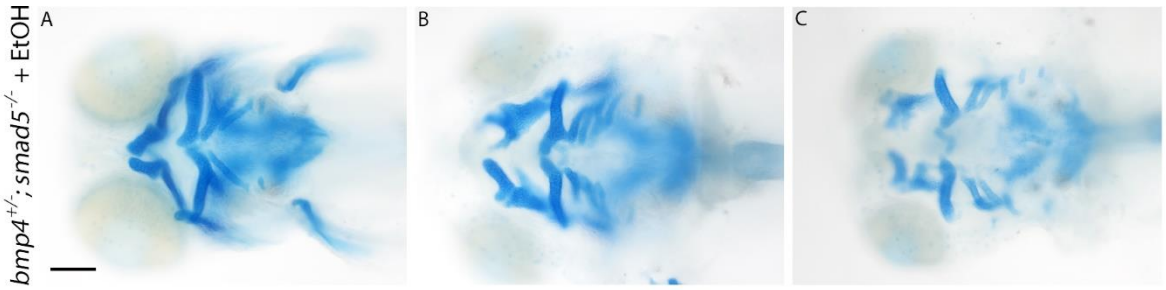


**Supplemental Figure 2. A wide spectrum of viscerocranial malformations was observed in ethanol-treated *bmp4*$^{+/-}$*;smad5*$^{-/-}$ larvae.** (**A-C**) Whole-mount images of viscerocranium at 5 dpf larvae. Cartilage is blue and bone is red (Ventral views, anterior to the left, scale bar: 100 µm). (**A-C**) Ethanol exposure on *bmp4*$^{+/-}$*;smad5*$^{-/-}$ larvae range from stereotypical *smad5* mutant phenotypes to severe ethanol-induced phenotypes to the viscerocranium.

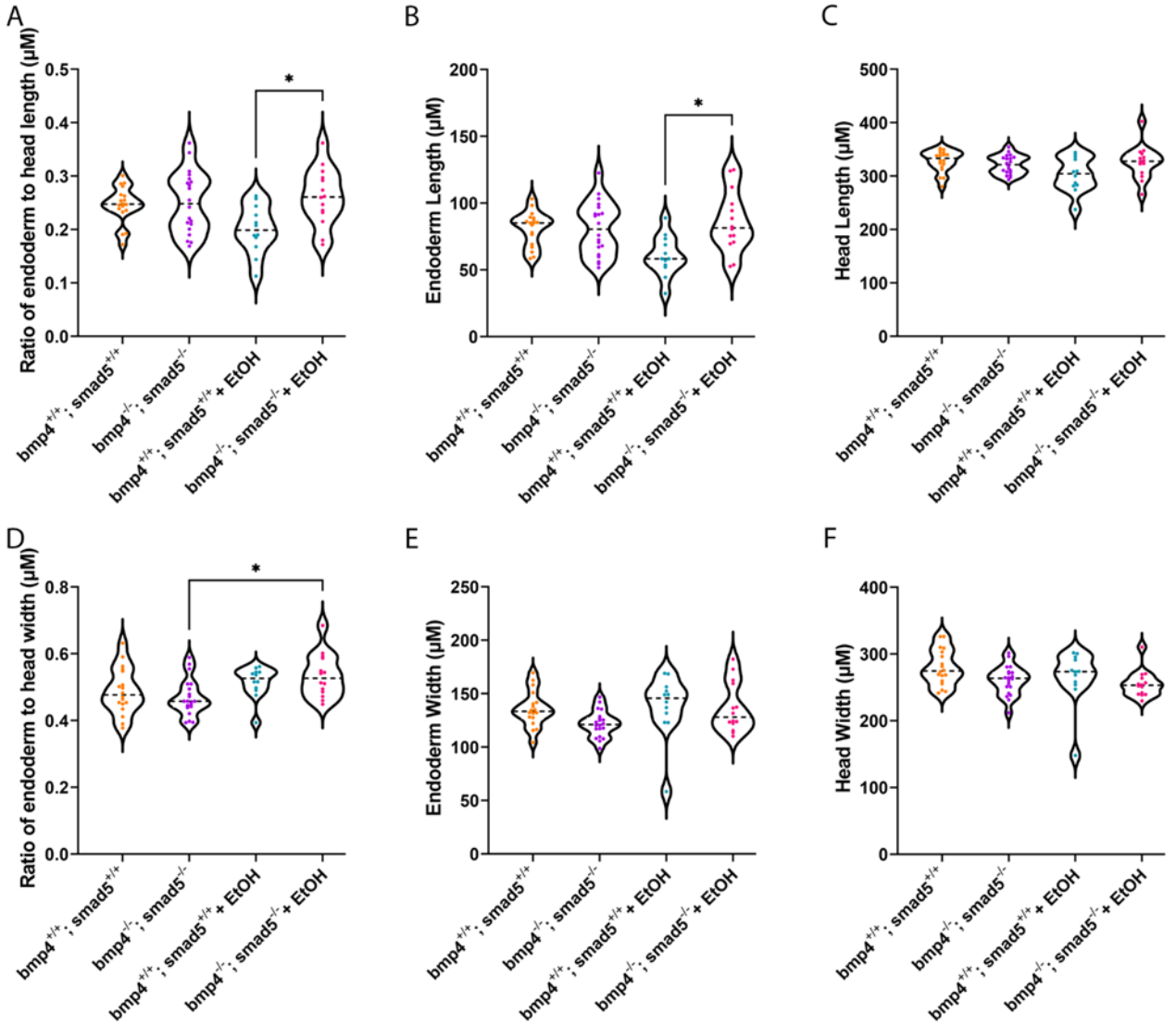


**Supplemental Figure 3. Ethanol exposure alters size of the anterior pharyngeal endoderm in *bmp4$^{+/-}$;smad5$^{-/-}$* embryos.** (**A-F**) Length and width measures of the anterior pharyngeal endoderm. (**A-C**) Ethanol exposure decreased endoderm length but not head length in *bmp4$^{+/+}$;smad5$^{+/+}$* embryos but significantly increased endoderm length ethanol-treated *bmp4$^{-/-}$;smad5$^{-/-}$* embryos. (**D-F**) Ethanol-treatment significantly increased in the ratio of endoderm width to head width in *bmp4$^{-/-}$;smad5$^{-/-}$* embryos, though there was a trend in the increase in ethanol-treated *bmp4$^{+/+}$;smad5$^{+/+}$* embryos as well, but not in head width (individual graph statistics in Supplemental Table 1).

**Supplemental Table 1. Statistics for Supplemental Figure 3**

| Ratio of Endoderm to Head Length | | Endoderm Length | | Head Length | |
|---|---|---|---|---|---|
| **ANOVA** | F = 2.930 P = 0.0448 | **ANOVA** | F = 3.811 P = 0.0169 | **ANOVA** | F = 2.309 P = 0.0906 |
| **Tukey's Comparisons** | | **Tukey's Comparisons** | | **Tukey's Comparisons** | |
| *bmp4*$^{+/+}$;*smad5*$^{+/+}$ vs *bmp4*$^{-/-}$;*smad5*$^{+/+}$ | p = 0.9989 | *bmp4*$^{+/+}$;*smad5*$^{+/+}$ vs *bmp4*$^{-/-}$;*smad5*$^{+/+}$ | p = 0.8751 | *bmp4*$^{+/+}$;*smad5*$^{+/+}$ vs *bmp4*$^{-/-}$;*smad5*$^{+/+}$ | p = 0.3505 |
| *bmp4*$^{+/+}$;*smad5*$^{+/+}$ vs *bmp4*$^{+/+-}$;*smad5*$^{+/+}$ + EtOH | p = 0.8727 | *bmp4*$^{+/+}$;*smad5*$^{+/+}$ vs *bmp4*$^{+/+-}$;*smad5*$^{+/+}$ + EtOH | p = 0.8751 | *bmp4*$^{+/+}$;*smad5*$^{+/+}$ vs *bmp4*$^{+/+-}$;*smad5*$^{+/+}$ + EtOH | p = 0.1492 |
| *bmp4*$^{+/+}$;*smad5*$^{+/+}$ vs *bmp4*$^{-/-}$;*smad5*$^{-/-}$ + EtOH | p = 0.0127 | *bmp4*$^{+/+}$;*smad5*$^{+/+}$ vs *bmp4*$^{-/-}$;*smad5*$^{-/-}$ + EtOH | p = 0.8751 | *bmp4*$^{+/+}$;*smad5*$^{+/+}$ vs *bmp4*$^{-/-}$;*smad5*$^{-/-}$ + EtOH | p = 0.2876 |
| *bmp4*$^{-/-}$;*smad5*$^{-/-}$ vs *bmp4*$^{+/+}$;*smad5*$^{+/+}$ + EtOH | p = 0.9211 | *bmp4*$^{-/-}$;*smad5*$^{-/-}$ vs *bmp4*$^{+/+}$;*smad5*$^{+/+}$ + EtOH | p = 0.8751 | *bmp4*$^{-/-}$;*smad5*$^{-/-}$ vs *bmp4*$^{+/+}$;*smad5*$^{+/+}$ + EtOH | p = 0.8835 |
| *bmp4*$^{-/-}$;*smad5*$^{-/-}$ vs *bmp4*$^{-/-}$;*smad5*$^{-/-}$ + EtOH | p = 0.0089 | *bmp4*$^{-/-}$;*smad5*$^{-/-}$ vs *bmp4*$^{-/-}$;*smad5*$^{-/-}$ + EtOH | p = 0.1277 | *bmp4*$^{-/-}$;*smad5*$^{-/-}$ vs *bmp4*$^{-/-}$;*smad5*$^{-/-}$ + EtOH | p = 0.992 |
| *bmp4*$^{-/-}$;*smad5*$^{-/-}$ + EtOH vs *bmp4*$^{-/-}$;*smad5*$^{-/-}$ + EtOH | p = 0.0033 | *bmp4*$^{-/-}$;*smad5*$^{-/-}$ + EtOH vs *bmp4*$^{-/-}$;*smad5*$^{-/-}$ + EtOH | p = 0.0494 | *bmp4*$^{-/-}$;*smad5*$^{-/-}$ + EtOH vs *bmp4*$^{-/-}$;*smad5*$^{-/-}$ + EtOH | p = 0.9686 |
| **Ratio of Endoderm to Head Width** | | **Endoderm Width** | | **Head Width** | |
| **ANOVA** | F = 3.063 P = 0.0386 | **ANOVA** | F = 1.869 P = 0.1499 | **ANOVA** | F = 2.691 P = 0.0587 |
| **Tukey's Comparisons** | | **Tukey's Comparisons** | | **Tukey's Comparisons** | |
| *bmp4*$^{+/+}$;*smad5*$^{+/+}$ vs *bmp4*$^{-/-}$;*smad5*$^{+/+}$ | p = 0.8133 | *bmp4*$^{+/+}$;*smad5*$^{+/+}$ vs *bmp4*$^{-/-}$;*smad5*$^{+/+}$ | p = 0.2316 | *bmp4*$^{+/+}$;*smad5*$^{+/+}$ vs *bmp4*$^{-/-}$;*smad5*$^{+/+}$ | p = 0.1886 |
| *bmp4*$^{+/+}$;*smad5*$^{+/+}$ vs *bmp4*$^{+/+-}$;*smad5*$^{+/+}$ + EtOH | p = 0.652 | *bmp4*$^{+/+}$;*smad5*$^{+/+}$ vs *bmp4*$^{+/+-}$;*smad5*$^{+/+}$ + EtOH | p = 0.9983 | *bmp4*$^{+/+}$;*smad5*$^{+/+}$ vs *bmp4*$^{+/+-}$;*smad5*$^{+/+}$ + EtOH | p = 0.3263 |
| *bmp4*$^{+/+}$;*smad5*$^{+/+}$ vs *bmp4*$^{-/-}$;*smad5*$^{-/-}$ + EtOH | p = 0.1846 | *bmp4*$^{+/+}$;*smad5*$^{+/+}$ vs *bmp4*$^{-/-}$;*smad5*$^{-/-}$ + EtOH | p = 0.9993 | *bmp4*$^{+/+}$;*smad5*$^{+/+}$ vs *bmp4*$^{-/-}$;*smad5*$^{-/-}$ + EtOH | p = 0.0523 |
| *bmp4*$^{-/-}$;*smad5*$^{-/-}$ vs *bmp4*$^{+/+}$;*smad5*$^{+/+}$ + EtOH | p = 0.2343 | *bmp4*$^{-/-}$;*smad5*$^{-/-}$ vs *bmp4*$^{+/+}$;*smad5*$^{+/+}$ + EtOH | p = 0.277 | *bmp4*$^{-/-}$;*smad5*$^{-/-}$ vs *bmp4*$^{+/+}$;*smad5*$^{+/+}$ + EtOH | p > 0.9999 |
| *bmp4*$^{-/-}$;*smad5*$^{-/-}$ vs *bmp4*$^{-/-}$;*smad5*$^{-/-}$ + EtOH | p = 0.0324 | *bmp4*$^{-/-}$;*smad5*$^{-/-}$ vs *bmp4*$^{-/-}$;*smad5*$^{-/-}$ + EtOH | p = 0.2553 | *bmp4*$^{-/-}$;*smad5*$^{-/-}$ vs *bmp4*$^{-/-}$;*smad5*$^{-/-}$ + EtOH | p = 0.8529 |
| *bmp4*$^{-/-}$;*smad5*$^{-/-}$ + EtOH vs *bmp4*$^{-/-}$;*smad5*$^{-/-}$ + EtOH | p = 0.8716 | *bmp4*$^{-/-}$;*smad5*$^{-/-}$ + EtOH vs *bmp4*$^{-/-}$;*smad5*$^{-/-}$ + EtOH | p > 0.9999 | *bmp4*$^{-/-}$;*smad5*$^{-/-}$ + EtOH vs *bmp4*$^{-/-}$;*smad5*$^{-/-}$ + EtOH | p = 0.866 |

**Supplemental Table 1. Statistical analyses of linear anterior endoderm/head measures in Supplemental Figure 3.** Linear measures of anterior endoderm/head were analyzed with a two-way ANOVA (type III). F-statistic and P-value for each analysis are shown. A Tukey's Multiple Comparisons Test for each comparison are shown.

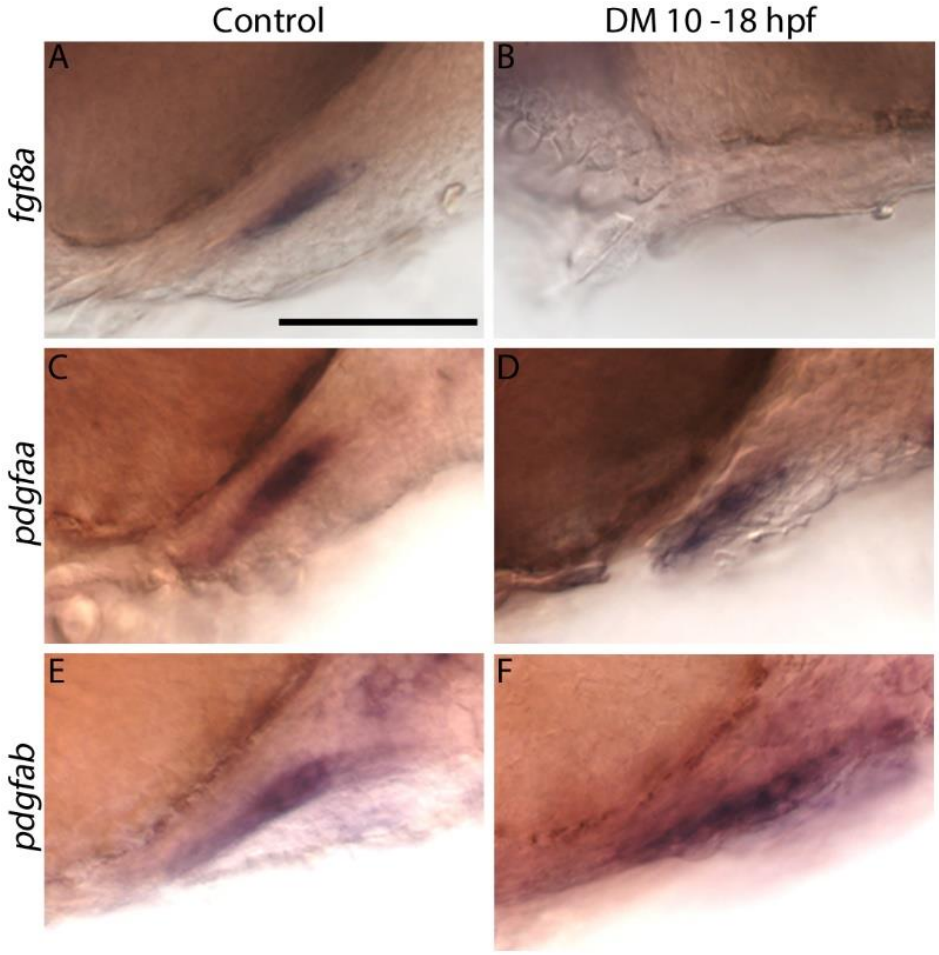


881

882 **Supplemental Figure 4. Ethanol exposure changes shape of oral ectoderm expression domain in *bmp4*$^{-/-}$*;smad5*$^{-/-}$**
883 **embryos.** (**A-F**) Whole-mount images of untreated and Dorsomorphin-treated embryos labeling *fgf8a, pdgraa* and
884 *pdgfab* gene expression at 36 hpf (lateral views, anterior to the left, scale bar: 50 µm). (**A,C,E**) Normal expression of
885 *fgf8a, pdgfaa* and *pdgfab* in the oral ectoderm of untreated embryos. (**B, D, F**) Expression of *fgf8a* is lost in
886 Dorsomorphin-treated embryos, while *pdgfaa* and *pdgfab* are expressed normally (n = 20 embryos per group).